CFD SIMULATION FOR THE EROSION ON ELECTRICAL SUBMERSIBLE PUMP DUE TO VISCOSITY AND AIR PRESENCE

A Thesis

by

BAHADIR BASARAN

Submitted to the Office of Graduate and Professional Studies of
Texas A&M University
in partial fulfillment of the requirements for the degree of

MASTER OF SCIENCE

Chair of Committee,	Gerald L. Morrison
Committee Members,	Michael B. Pate
	Robert E. Randall
Head of Department,	Andreas A. Polycarpou

May 2017

Major Subject: Mechanical Engineering

ABSTRACT

There is a necessity to use artificial lift when the natural drive of oil is not strong enough to push the oil from the well bottom to the surface. Electrical Submersible Pump (ESP) systems have been used far and wide by the petroleum industry to compensate the need of lift. The pump part of an ESP system needs to deal with the erosion due to both slurry working conditions and the presence of air. Presence of abrasive particles can erode hydraulic as well as secondary flow paths which can lead to damage of the pump resulting in affects ranging from performance degradation to pump failure.

This study is focused on CFD (Computational Fluid Dynamic) based evaluation of erosion in ESP pump section under different operating conditions. The pump was modelled at 3600 rpm at best efficiency point for different viscosities such as 1 cp, 5cp, 20cp and 60cp. Two gram/liter of sand was introduced at the inlet of the pump. Eulerian approach was utilized to model the two phase flow simulation using ANSYS Fluent. An erosion model developed in the Turbomachinery lab for the pump was utilized to predict the erosion. The developed equation was compared with inbuilt ANSYS erosion prediction equations using the DPM approach. Erosion rates as a function of viscosity across different sections of the pump were obtained and compared with previously published data.

From the previous erosion testing of ESPs, it is learned that erosion rates accelerated in the presence of gas. The CFD study was undertaken to evaluate the effect of gas presence on erosion rates. The two phase flow simulation was conducted to

evaluate the effect of bubble size on flow separation and pump performance. A three phase flow simulation was performed for the first time using 850gpm water, 15 % GVF (Gas Void Fraction) of air and 2grams/liter of sand. The study concludes with a discussion about the effect of bubble size on phase separation erosion modeling in presence of gas and potential improvement required to calibrate the three phase flow simulation.

ACKNOWLEDGEMENTS

I would like to first say a very big thank you to my advisor Professor Gerald L. Morrison for his support and inspiration on my work. He provided a good teaching, good company and many of great advices throughout my studies

I would like to thank my committee members, Dr. Robert E. Randall and Dr. Michael Pate for their guidance throughout the course of this research.

Tons of thanks to Dr. Abhay Patil and Yiming Chen for their limitless helps and patience on my work.

Thanks also go to my friends, colleagues and the department faculty and staff for making my time at Texas A&M University a great experience. I also want to extend my gratitude to my colleagues at Turbomachinery Lab, Burak C. Ayyildiz, Changrui Bai, Rahul Agarwal, Wenfei Zhang, Wenjie Yin, Yi Chen, Yintao Wang for always being a great company.

Lastly, and most importantly, thanks to my parents and my dear sister for their encouragement and patience.

NOMENCLATURE

AGH	Advanced gas handler
BPD	Barrels per day
CFD	Computational fluid dynamics
D	Diameter
DPM	Discrete phase model
DOE	Design of experiments
D_h	Hydraulic diameter
E/CRC	Erosion-Corrosion research center
EF	Erosion factor
ER	Erosion rate
ESP	Electric submersible pump
GVF	Gas volume fraction
GPM	Gallons per minute
H	Head
HP	Horsepower
k_w	Turbulent kinetic energy
$\overline{k_{w_0}}$	Reference turbulent kinetic energy
Re	Reynolds number
rpm	Revolution per minute
TKE	Turbulent kinetic energy

V_s	Near wall sand velocity
$\overline{V_{s_0}}$	Reference sand velocity
$\boldsymbol{\rho}$	Density
ɥ	Viscosity
η	Pump efficiency
Φ	Flow rate coefficient
Ψ	Head coefficient
α_s	Sand concentration

TABLE OF CONTENTS

Page

LIST OF FIGURES

Page

LIST OF TABLES

Page

1. INTRODUCTION

The majority of oil wells flow naturally from the well bottom to the surface during early periods of their lives. After a certain amount of time, oil production rate decreases and wells die; at this point, a reservoir lacks satisfactory drive to provide flows at high rates. Artificial lift is a common technique used to obtain the desired flow rate of oil production from the well by increasing the bottom hole pressure. In other words, there is a need for an artificial lift when the natural drive of the oil is not strong enough to push the oil from bottom to the surface [1].

Electrical Submersible Pump (ESP) systems have been used far and wide by the petroleum industry to provide the needed additional lift. The working principle of the modern ESP was invented by Armais Sergeevich Arutunoff in 1927, and since then, the components of ESP have experienced a nonstop improvement throughout the long years. Today, more than 140,000 ESP systems are in service for both on-shore and off-shore fields all over the world. By 2015, ESP stands in second place after beam (rod) pumps in terms of oil production methods. Table 1 shows the comparison of the well-known artificial lift methods[2].

Table 1 Global Artificial Lift Choices [2]

Artificial Lift Method	Maximum Depth (ft)	Typical Operating Volume (bbl/d)	Worldwide Number of Wells
Beam Pump	16,000	0 to 1,000	600,000
Electric Submersible Pump	15,000	400 to 60,000	146,700
Gas Lift	18,000	100 to 80,000	48,300
Progressive Cavity Pump	8,600	0 to 5,000	31,500

A typical ESP system shown in Figure 1 contains both surface mechanisms and underground mechanisms.

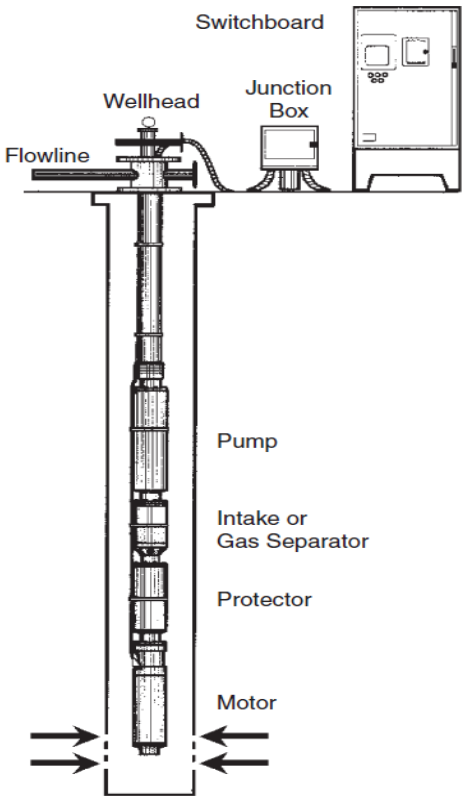

Figure 1 Classic ESP System [3]

For a classic ESP system, the main components of the downhole equipment consists of an ESP motor, the protector or seal section, gas separator, submersible pump and ESP cable. Surface equipment contains wellhead, junction box, switchboard, transformers, and surface cables. Over the decades, the design criteria and working properties of both downhole and surface equipment have been significantly improved; however the basic working principle is still the same as when it was invented.

Main features that make ESP installation conventional are:

- On ESP installations, produced liquid viscosity is low, converging to water viscosity.
- Inlet of the centrifugal pump consists of only liquid without free gases to provide ideal conditions for the pump. Low volumes of free gases which are produced by the well can be present at the pump suction zone. These gases can be moved away by the gas separator.
- Rotational velocity of centrifugal pump remains the same during processes due to the ESP motor is powered by a constant frequency drive. Variable frequency drives are becoming more common changing this feature.

Huge variations of field conditions are viable for the conventional ESP installation even if the given situations are not satisfied all the time. Common advantages of using ESP system in oil industry are given as [1, 4],

- Good operating efficiency for high production wells
- Feasible for various field conditions
- Reduced maintenance cost due to low repair frequency

- There is no well depth restriction.

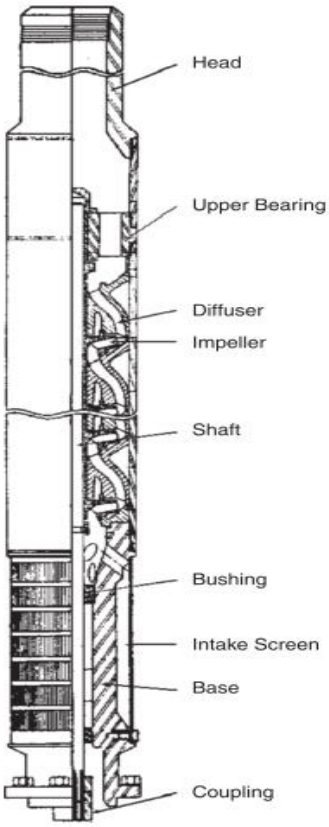

Figure 2 Electric Submersible Pump Parts [3]

A single stage of the ESP is shown in Figure 2. Submersible pumps are the keystone component of ESP. A multistage set of centrifugal pumps play a crucial role to obtain needed flow rates. Each stage consists of an impeller and diffuser, which are the components that provide high pressure flow in the well. Fluid enters the impeller which is rotating at high speed; velocity and kinetic energy of fluid dramatically increases in this section. In the diffuser, which is a stationary part of stage, the kinetic energy of the

fluid is converted into pressure energy. Then the fluid moves to the entrance of the next stage. This process repeats until the working fluid arrives at the pump discharge after passing through all the stages.

As a dynamic displacement pump, the fluid production rate of ESP devices change with respect to produced pressure force. The main factors which effect the fluid production rate of an ESP pump are,

- The distance from pump to surface(actual head)
- Impeller design(diameter)
- Electric motor current/frequency (effects rotational speed)
- Liquid properties[3]

1.1 Experimental and Theoretical Studies

Previously, modelling multiphase flow inside a pump was not an easy task due to the complexity of flow behavior; consequently, series of experiments were carried out at the University of Tulsa to establish empirical data on ESPs. Pessoa and Prado [5], performed a study focused on degradation of pump performance due to presence of gas variation. Using water and air as working fluids for a 22 stage pump system, they performed the experiments for both single (water) and two phase (water-air) flows. Surging and gas locking conditions were the key points as well as to observe head degradation due to existence of air. Surging is a term associated with the instability of pump, which effects head performance and is dependent on bubble pattern in the flow, which causes pressure fluctuations. Under two-phase flow condition, the gradual head

degradations in ESPs are subtle before there is an observation of instantaneous performance failure in the pump head. Surging occurs in this critical situation[6].Gas lock is the condition when a pump stops transferring head. In the gas lock condition, amplifying the intake pressure can help to bring pump back in ordinary working condition. After obtaining the head curve of the pump from experiments, they compared obtained results with the presented catalog specifications of pump. The difference between experiments and catalog specifications increased with increasing amounts of air. They pointed out that there is a requirement of an all-purpose model to estimate ESP performance for two phase flow[5].

Lea and Bearden [7] worked on three different kinds of ESPs named I-42B and C-72(radial), and K-70(mixed). Two phase flow was obtained using diesel and CO_2. I-42B was also set for water and air two-phase flow. The maximum number of stages was eight. Tests were repeated under low pressures by increasing gas fraction until the pump was not able to deliver the head. Regarding this study, results showed that the radial stage pumps were not able to give satisfying heads as well as mixed-flow impeller pumps. There was a noticeable drop in pump performance when gas volume fraction was more than 10%[7].

Turpin, Lea and Bearden [8] also worked on the I-42B and K-70 pumps and established practical correlations for calculating the head curve as a function of gas-liquid ratio and pressure. For three different gas volume fractions, obtained heads were plotted as seen in Figure 3.

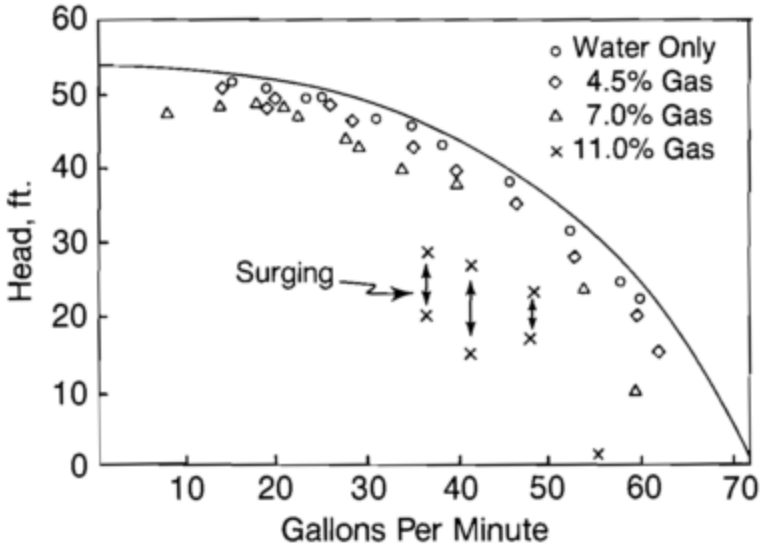

Figure 3 Water-Air Head Curve [8]

Head curve graphics and mathematical relations for two-phase flow were obtained. Head drop with increasing GVF was observed. Generated head and deterioration parameters for both I-42B and K-70 pumps were used to obtain empirical correlations.[8]

Cirilo [9] obtained two phase air-water flow performance curves of different types of submersible pumps including both radial and mixed flow pumps. For all pump types it was observed that increasing pressure at the inlet improved the ability of the pump to handling free gas. The effect of free gas played a vital role at lower rates of liquid flow. Frequency was increased to see the effect of rotation speed. A small enhancement was observed in terms of handling with gas by increasing frequency. Another result from this study showed the effect of stage numbers on centrifugal pumps.

As seen from Figure 4, head production was improved by increasing the number of stages.

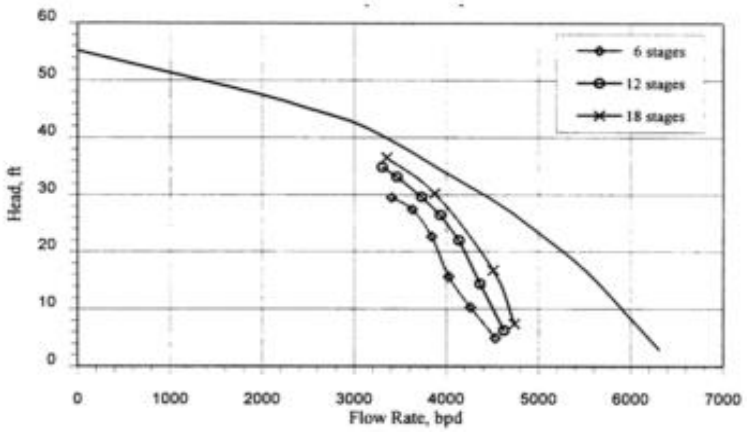

Figure 4 Pump Performance with Different Number of Stages, GVF: 15% [9]

Minemura and Murakami [10] used numerical approaches for a radial flow impeller and made a comparison with experimental data. Investigating the effects of cavitation on erosion problems was the aim of their study. In order to identify the rotation of air bubbles around the impeller, air bubbles with small radius were inserted into the flow zone and motion equations were applied. Assuming the water flow in the impeller is steady and inviscid; equations of motion were solved numerically to detect the trajectory of bubbles inside the water flow. Computer software was used for the calculation of flow field. Air bubbles in the flow zone were recorded experimentally by high speed cameras for confirmation. Numerical results showed a good agreement with experimental data. Results showed air bubble size was an important factor on inertial forces. When air bubble size diameter was increased, impact of the inertial forces on the

rotational motion was also increased. In this research, negative effects of increasing bubble diameter on the flow regime was shown by mathematical calculations in terms of inertial forces[10].

1.2 Numerical Studies for Single Phase Flow

In order to observe the complicated flow structure in a centrifugal pump, research was conducted by Cheah, Lee, Winoto and Zhao [11] . The aim of the study was modeling the flow inside a six-blade impeller. Using 1450 rpm rotation speed, the simulation was repeated for various mass flow rates at the inlet boundary. Unstructured tetrahedral elements were used for meshing. For numerical analysis, a commercial program CFX was used with standard k-Ɛ turbulence model. The pressure visualization of the internal flow inside the pump was obtained. Comparison between experimental and computational data was observed. By improving the mesh quality, numerical calculations repeated. Figure 5 shows the comparison of experimental data and numerical analysis results.

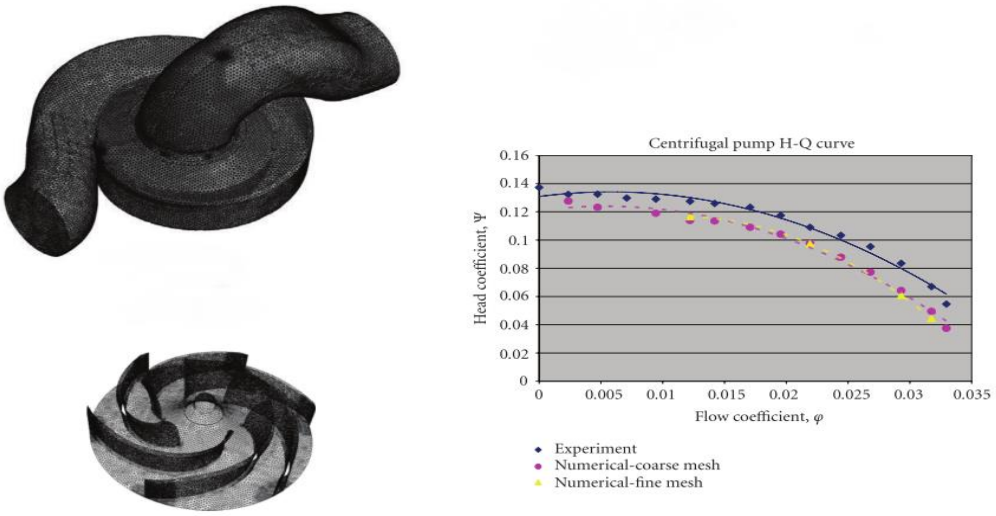

Figure 5 Mesh Structure and Comparison of Experimental and Numerical Results [11]

Data of efficiency, predicted head and pressure distribution were obtained from the CFD software program. Also, increasing mesh quality did not play an effective role to obtain a closer agreement with experimental data.

Research that helps to understand the contribution of numerical analysis to estimate water pump performance was done by González, Fernández, Blanco and Santolaria [12]. Due to the sophistication of 3D flow through centrifugal pumps, the authors stated that there was a need for numerical calculation to predict centrifugal pump performance. For the experimental part of the research, pressure distributions for single phase fluid on the impeller blades, with respect to various flow rates, are measured by sensors. For the numerical simulation, a sliding mesh method was applied and the 3D Navier-Stokes equation for incompressible flow was considered as a mathematical model. Standard k-Ɛ model was used in order to model the turbulent flow. Flow rate

distributions at the inlet and outlet sections were inserted as boundary conditions. Figure 6 shows the pressure distribution on the centrifugal pump.

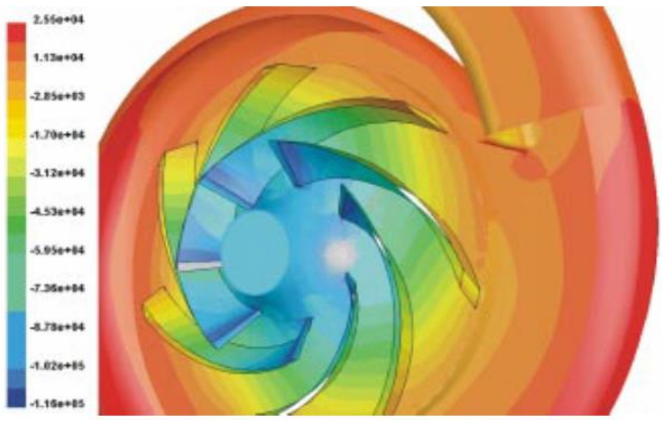

Figure 6 Static Pressure Contours by Numerical Analysis [12]

Compared results of experimental observation and numerical analysis were obtained and illustrated in Figure 7. Ψ is the head coefficient, Φ is the flow coefficient, and η is the pump efficiency for the figures below.

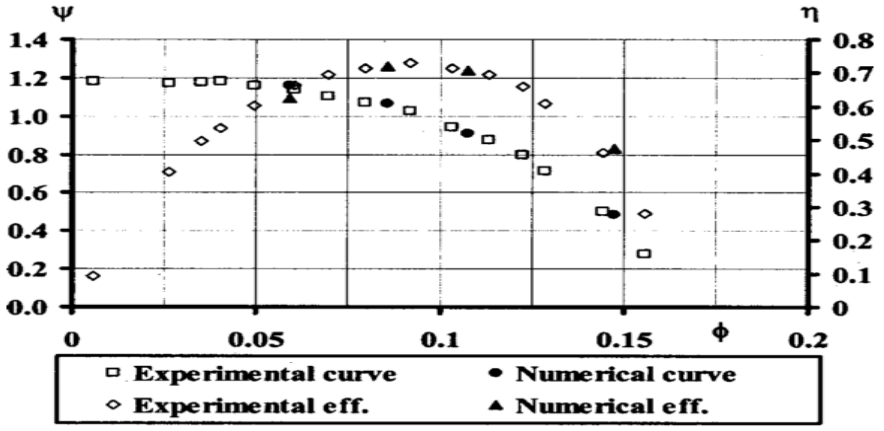

Figure 7 Performance Comparison of Numerical and Experimental Results [12]

For the CFD part, different flow rates were used to visualize the accuracy of analysis. A non-dimensional magnitude $\frac{P_a}{\frac{1}{2}\rho {U_2}^2}$ was plotted as a function of angular position, φ in order to compare pressure fluctuations. In Figure 8, flow rate is 0.7 times nominal flow rate, while it is 1.3 times greater in Figure 9.

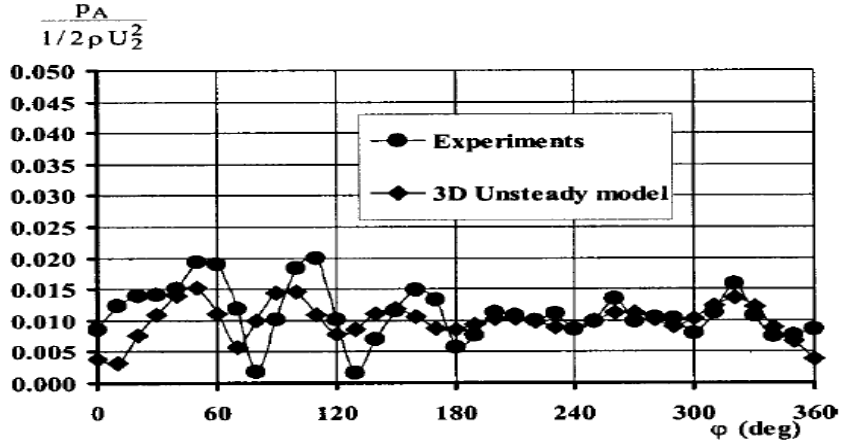

Figure 8 Pressure Fluctuations at the Impeller Blades for Low Speed (0.7 times nominal flow rate) [12]

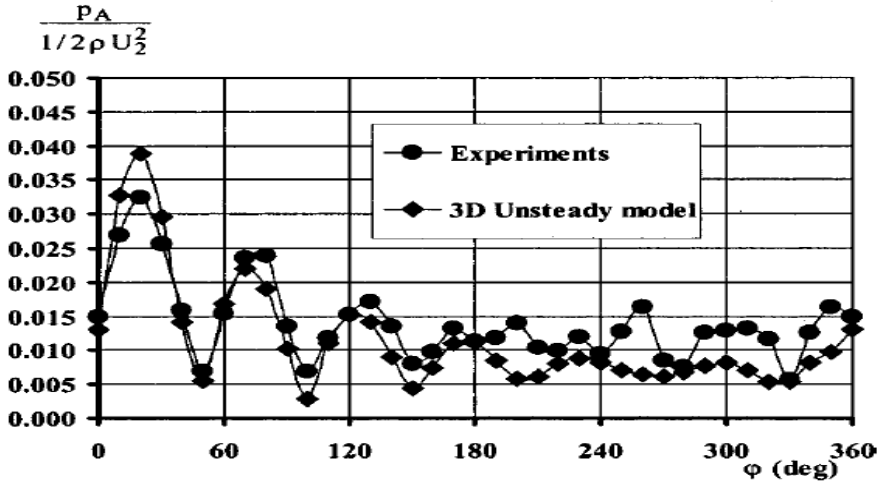

Figure 9 Pressure Fluctuations at the Impeller Blades for High Speed (1.3 times nominal flow rate) [12]

Obtained results from 3D numerical analysis and experiments are strongly consistent with each other [12].

An important study performed by Maitelli, Bezerra and Mata [13], which also applies CFD to centrifugal pumps. In this research, impeller, diffuser and the whole ESP geometry were modeled and numerical analysis was used to obtain performance curves. Figure 10 shows the views of the impeller, diffuser and the entire geometry.

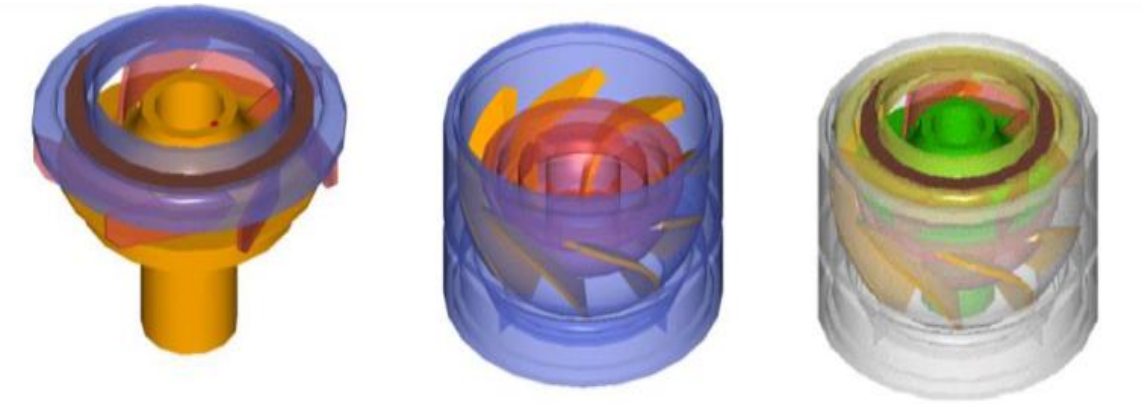

C1 C2 C3

Figure 10 3D Drawing of Impeller (C1), Entire Geometry (C2), and Entire Geometry with Extended Blades (C3) [13]

The entire geometry was divided into three main components; C1 which refers impeller, C2 refers impeller and diffuser, and C3 refers impeller and diffuser with extended blade size. The C3 region was modelled by researchers due to avoid convergence problems because of geometrical difficulties. ANSYS® CFX® release 11.0 was used as the commercial software, 3D simulations were applied based on numerical analysis methods. The k-Ɛ model was used for the turbulence solver. Single phase flow was modeled by water. For 3500 rpm speed of the impeller, ten different flow rates for each zone were modelled. The head curve of the pump was simulated for each condition and compared with the manufacturer's data as given in Figure 11.

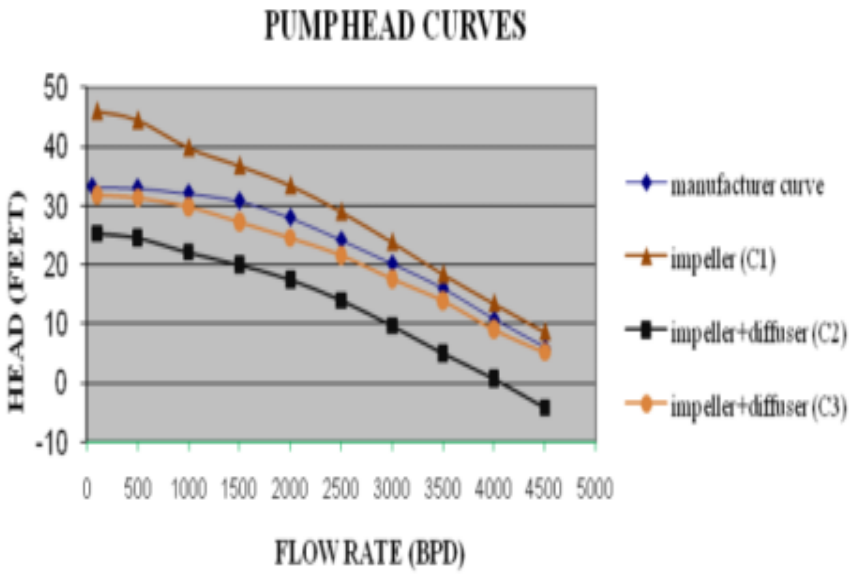

Figure 11 Comparison of Simulated Data and Manufacturer Head Curve [13]

Tendency of flow behavior obtained by CFD program is similar to manufacturer head curve for each zone. For C1, excessive head increase is observed at small flow rates. When the diffuser was also taken into account (C2), the excessive increase disappeared. Better results were obtained by improving geometry to overcome simulation difficulties (C3). In this study, CFD model showed a good agreement with the manufacturer's curve by making basic improvements on CFD simulation. It was concluded that CFD programs are reliable, time saving and cheap sources for the single phase flow modelling.

1.3 Numerical Studies for Multiphase Flow

For single phase flows, electrical submersible pumps are one of the most reliable systems to have a satisfactory performance. In an oil well, the existence of multiphase flow brings problems to pumps. The performance of an ESP degrades with the presence of gas. This degradation depends upon pump intake pressure and volume of gas in the system.

A study to understand the mechanism of air-water two phase flow was performed by Minemura, Uchiyama, Shoda and Egashira [14]. In this research, the mathematical background of centrifugal pump was compared with numerical analysis of centrifugal pump. Numerical analysis produced a fairly good result on shaft power and pump head within the range of 20 % difference of flow rate[14].

Beltur, Prado, Duran and Pessoa [15] conducted a two-phase flow behavior of ESP study to predict system performance. The aim of this study was predicting two-phase flow performance of an ESP using the Homogeneous Model. The primary fluid on this project was water, and air was used as the secondary fluid. Using results from experimental data, the head curve for a single-phase (water) flow was obtained. Experimental data was compared with obtained predicted performance by the Homogeneous Model. Performance curve of low viscosity fluid without free gas and with small amount of free gas values (<2%) mostly met with the performance curves provided by manufacturer.

When the free gas fraction was increased, homogeneous model was not usable on single-phase water performance curves to predict the performance of centrifugal pump due to surging and gas locking conditions.

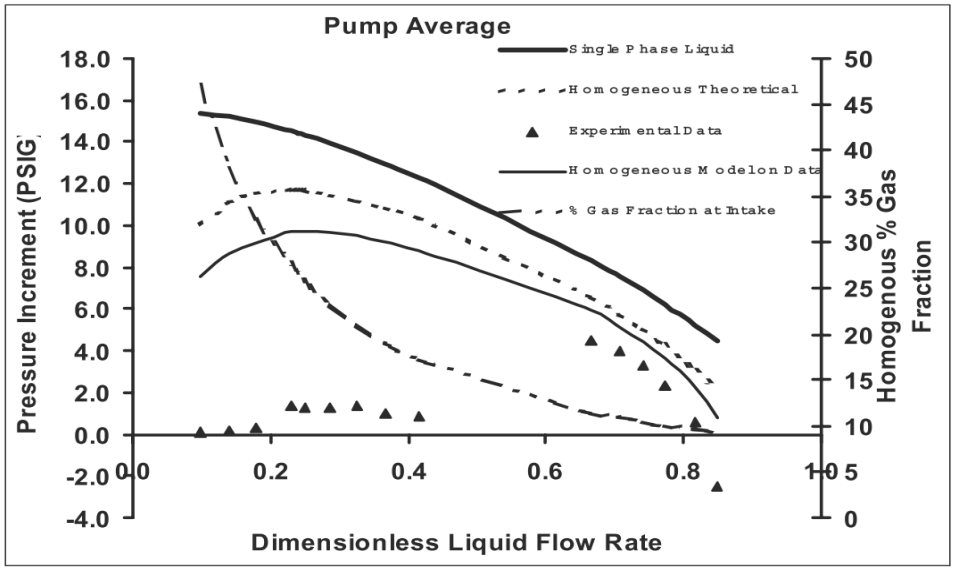

Figure 12 Comparison of Actual and Predicted Performances [15]

Figure 12 illustrates the differences of predicted head performance between the Homogeneous Model and experiments. The figure shows that there is a great deal of difference between two-phase flow head performance and single phase head performance. The authors concluded that in order to make a good correction on two-phase flow head performance using the Homogeneous Model, working parameters under gassy conditions must be known.[15]

In another study, Caridad, Asuaje, Kenyery, Tremante and Aguillón [16], indicated the effectiveness of ESP for multi-phase flow. Their study focused on the numerical simulations of two-phase flow on ESP impeller, including all stage analysis. They used water-air mixtures for simulations.

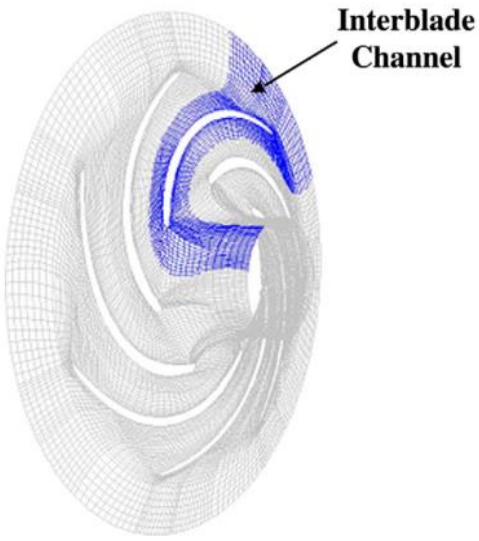

Figure 13 Impeller Geometry [16]

Using CFD commercial software, an Eulerian approach was used to visualize distribution of water and air. As a turbulence model, k-Ɛ model was selected according to suggestions based on the CFD software manual. The meshed domain of the impeller section is illustrated in Figure 13. Conditions of the simulation conditions are given Table 2.

Table 2 Simulation Conditions [16]

Domain	1 inter-blade channel(periodic condition)
Grid	27,552 elements
Inflow B.C.	Total pressure(100,000 Pa)
Outflow B.C.	Mass flow(variable)
Turbulence Model	k-Ɛ
Multiphase model	Two-fluid
Gas-Void Fraction (%)	0, 10, 15
Bubble diameter (mm)	0.1, 0.3, 0.5

Figure 15, which compares the results of experimental and simulated data for constant bubble diameter (0.1 mm), was obtained for single phase, 10% GVF and 15%GVF. When the figure on the left hand side shows the performance curve comparison for only the impeller, the figure on the right hand side illustrates the performance for an entire stage.

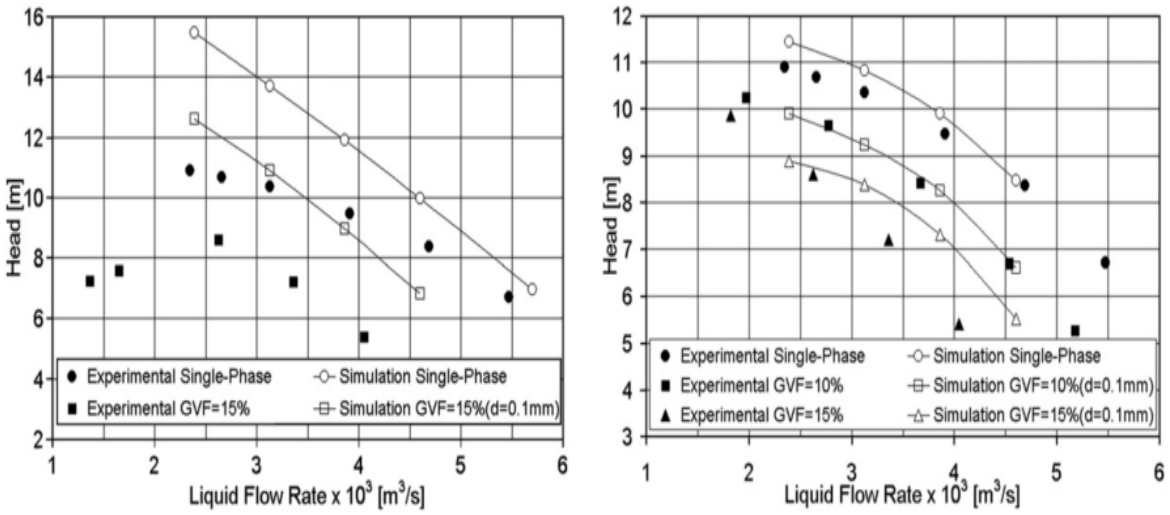

Figure 14 Comparisons of Simulated and Experimental Results [16]

From the comparison given in Figure 14, authors concluded that experimental and simulated results have a good agreement on impeller head gains with respect to liquid flow rate. Another important point recorded from this research is the effect of bubble size on the impeller head. For 15% GVF, single-phase and two-phase flows are modeled by CFD and results are compared in Figure 15.

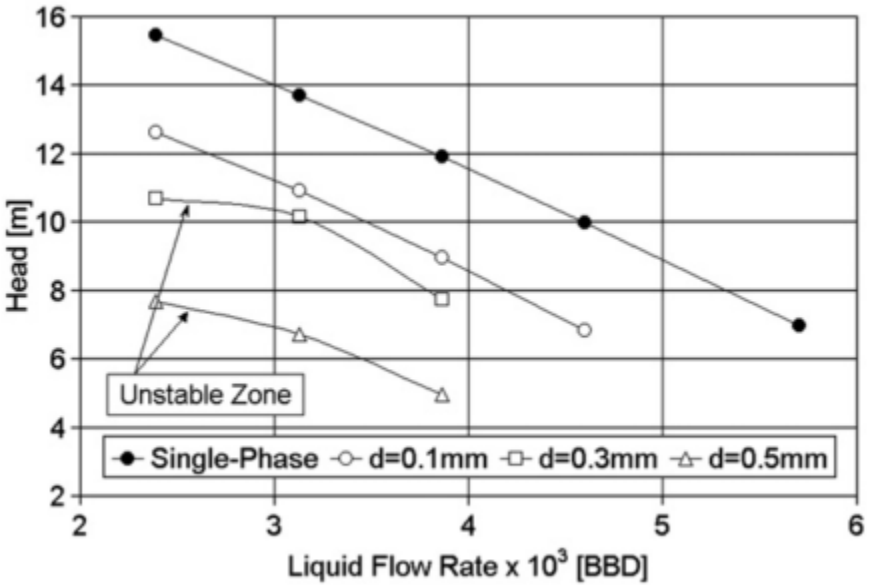

Figure 15 Bubble Size Effect on the Impeller Head [16]

In order to visualize the influence of bubble size, the flow with three different bubble diameters were modelled by CFD software. Results showed bubbles with larger diameter cause greater head losses. Another crucial point which stands out from Figure 15 is, for the diameter of 0.3 and 0.5 mm, the flow zone is unstable which causes the raise on hydraulic losses[16].

Qi,Turnquist and Ghasripoor [17]worked on a study to design ESP and develop a CFD analysis of designed ESP for geothermal utilizations. In their investigation, combining a one dimensional theoretical model, which is a set of formulas to determine design parameters in principle, with three dimensional numerical CFD analysis was used to form an advanced ESP design tool. Both single phase (water) flow and two-phase (water-air) flows were simulated. The procedure of pump design is shown in Figure 16.

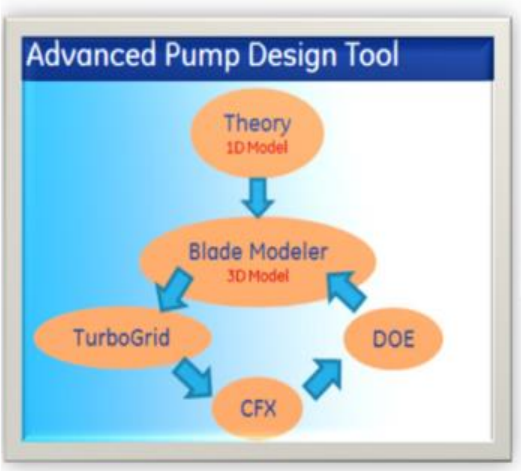

Figure 16 Pump Design Procedure[17]

At the first step, to characterize the proper style of impeller and specify blade size, one dimensional theoretical model was used by considering required pump performance parameters and operating conditions. Then, based on design parameters attained by one dimensional model, commercial software ANSYS BladeModeler was used to obtain three dimensional model. A mesh of the volute was obtained by TurboGrid. Then the meshed domain was sent to CFX for numerical CFD analysis. To

enhance the performance of the domain, Design of Experiments (DOE), which applies different impeller/diffuser design parameters and shows results for a simulated stage, was implemented to the tool. The ESP design scheme is shown in Figure 17.

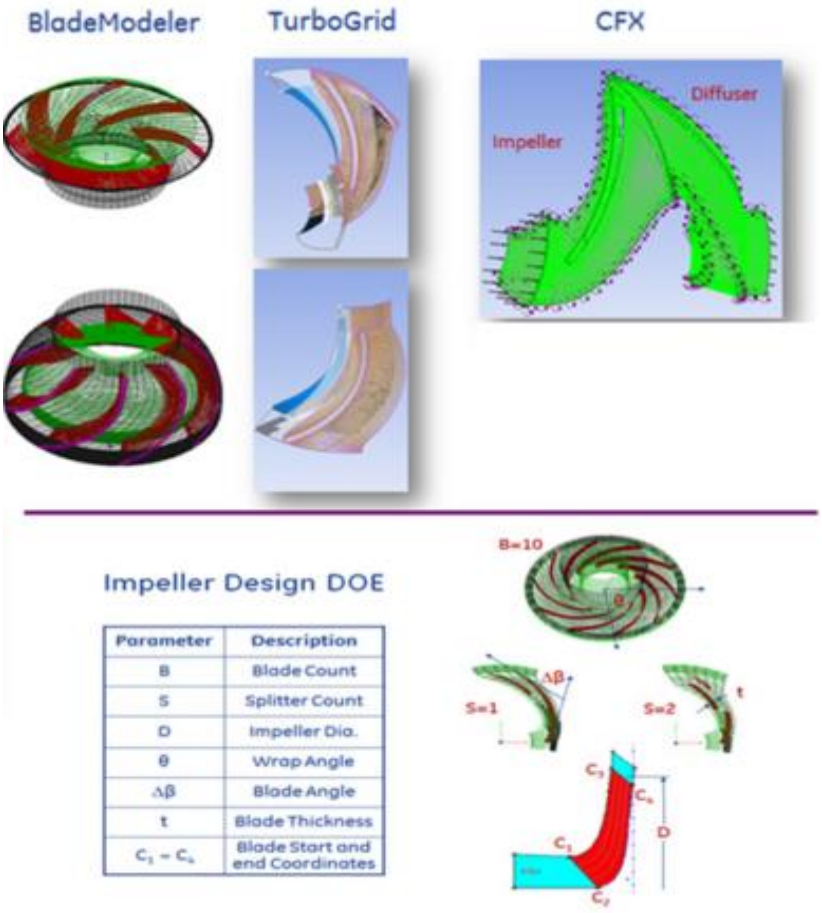

Figure 17 Pump Design Tool [17]

For the one dimensional model part, calibration was obtained by the results from a great numbers of experiments. Specific speed of the pump defined as:

$$N_S = \frac{N\sqrt{Q}}{(\Delta H)^{3/4}} \tag{1}$$

Where N_s is specific rotational speed, N is rotational speed, Q is flow rate, and H is head.

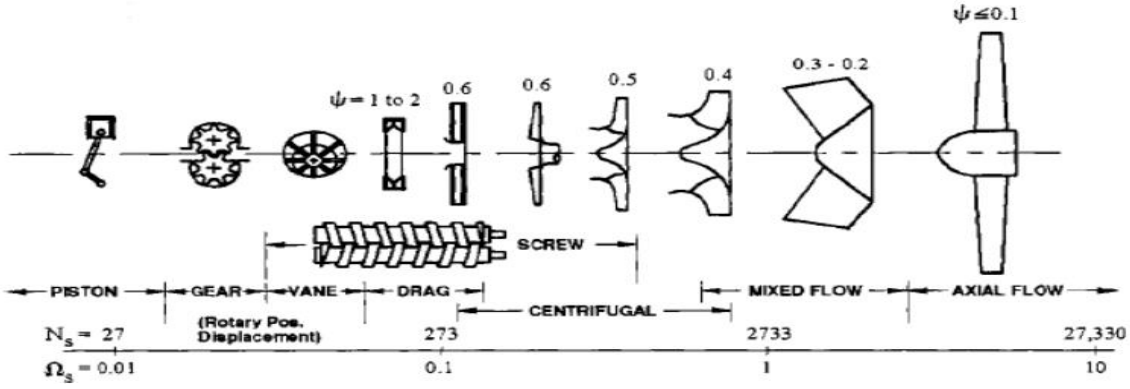

Figure 18 Geometry Selection for Various Specific Speeds [17]

Since the specific speed of an ESP is usually varies from 1000 to 5000, Radial Centrifugal, Francis Centrifugal and Mixed flow centrifugal pumps were considered to have a better pump efficiency with respect to Figure 18. After considering the working conditions, wellbore and ESP size limitations on geothermal applications, a mixed flow style centrifugal pump was picked from the list. Figure 19 illustrates the conceptual design of the pump which was modelled in BladeModeler.

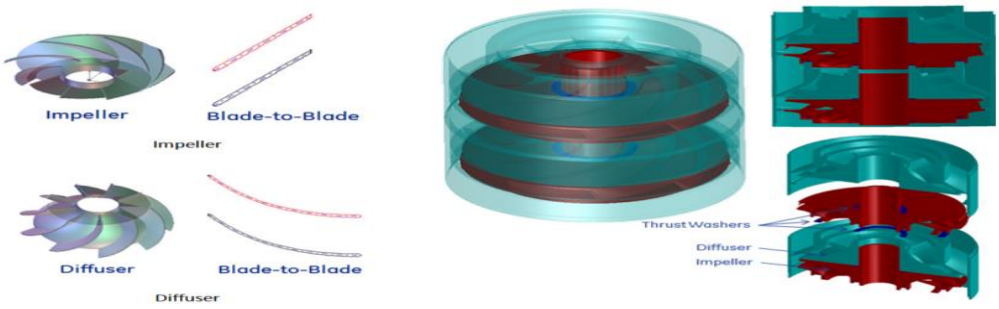

Figure 19 Design of Impeller/Diffuser and Stages (from left to right) [17]

Then, the meshed domain was created as given in Figure 20. A commercial software program ANSYS CFX5 Release 13 was performed to obtain CFD model.

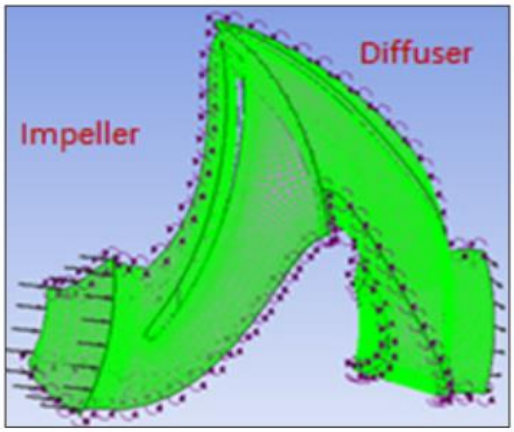

Figure 20 Fluid Domain Mesh [17]

Because of the symmetry and periodic distribution of blades, only one blade from diffuser and impeller were inserted to the program. Water at 300 °C was used as the operating fluid. For boundary conditions, 90 bar was defined as total pressure at the inlet. 80 kg/s mass flow rate was identified for outlet and all other parts defined as a wall

which is a default boundary condition by the commercial program. Standard k-Ɛ model was used to model the turbulent flow; each case converged after a few hundred time steps.

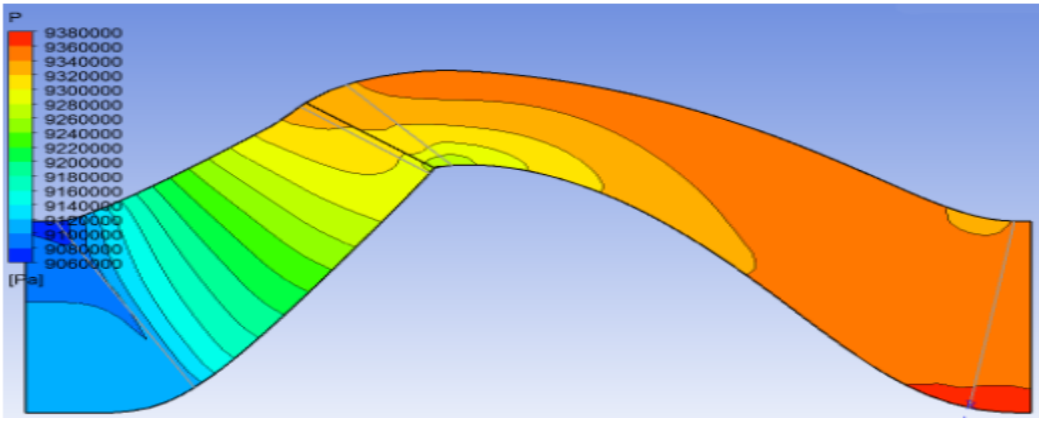

Figure 21 Static Pressure on Meridional Surface (from impeller to diffuser) [17]

Figure 21 is an illustration of the area averaged static pressure distribution from the impeller to the diffuser. The increment of static pressure was found as 250,000 Pa at the outlet, which produces 32m of static head increase. To increase the pump performance, DOE was applied with respect to some of important parameters like blade count, splitter count, vane angle, wrap angle, etc. After the application of DOE, the efficiency curve of the ESP is obtained shown in Figure 22.

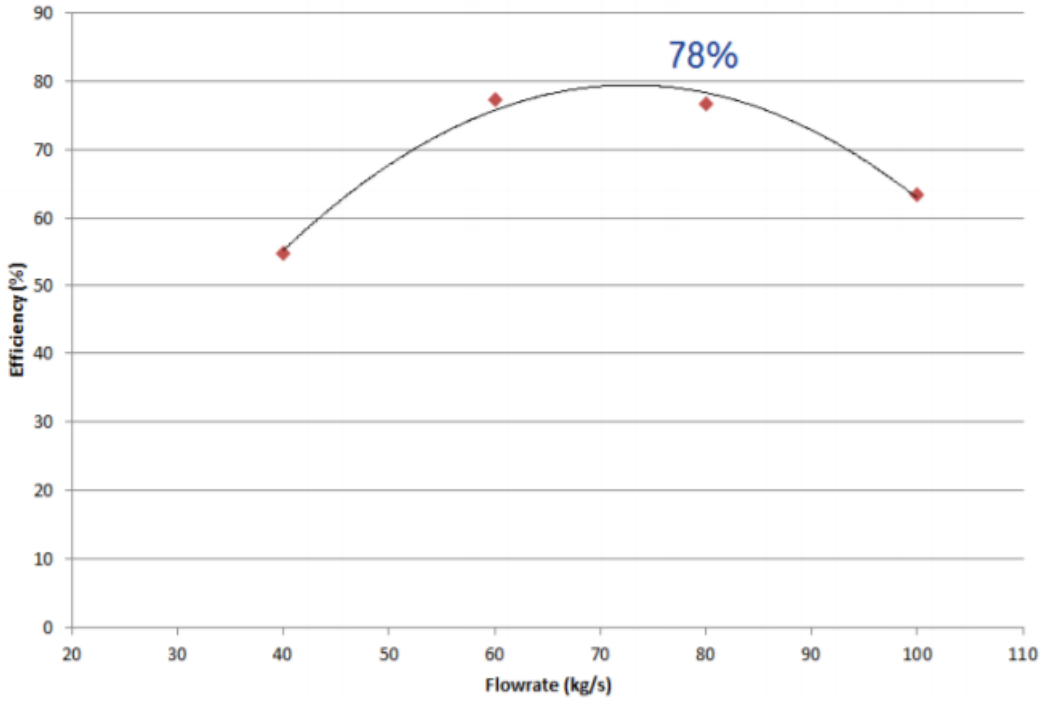

Figure 22 Curve of Efficiency [17]

For two-phase flow, the maximum gas volume fraction was limited to 2%. The other boundary conditions remained the same. No substantial air bubbles were observed on the blades, shroud and the hub parts of the ESP. There was a 1.8 % of static pressure drop, which can be assumed negligible, when compared to the single phase flow. These result showed that there was no need to provide any additional equipment for handling with 2% gas volume fractions. Air volume fractions for impeller hub, shroud and blades were plotted as seen in Figure 23.

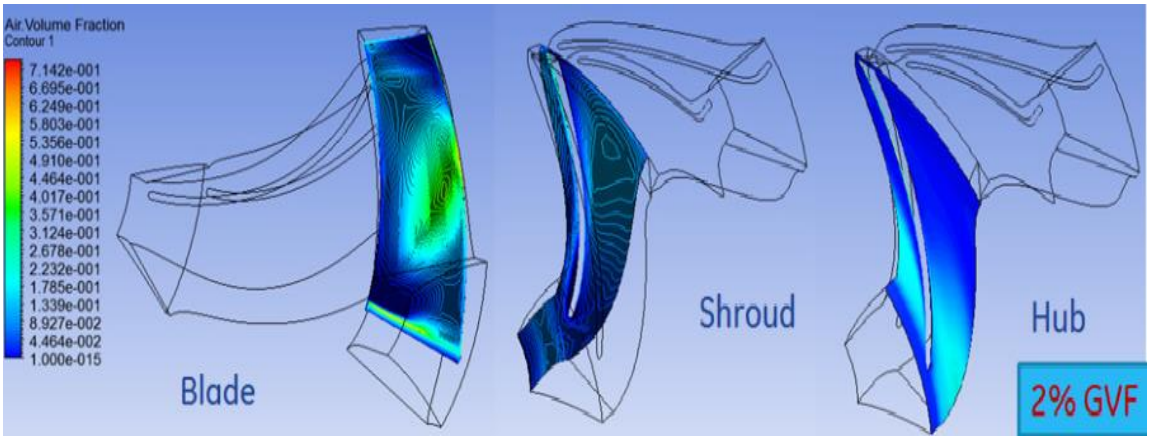

Figure 23 Air Volume Fraction Contours on Blade, Shroud and Hub [17]

To verify design process of the ESP, a comparison was made with an existing ESP which works under the same conditions with single phase simulated model.

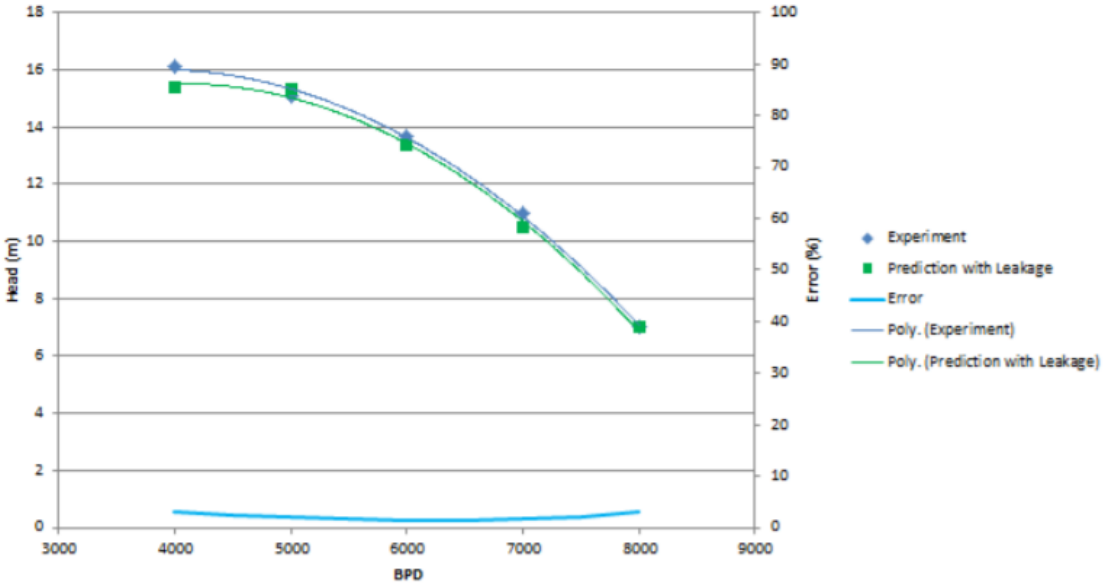

Figure 24 Obtained Head Comparison of CFD and Experimental Results [17]

Good agreement was obtained between the simulated case and experiments. As seen from Figure 24, obtained values of the head using the CFD analysis and experimental data was pretty close, which proves that implemented program was accurate and applicable to predict pump performance.

Marsis[18] performed two phase flow modeling on split vane pump impeller at 0, 10 20% GVF. Patil[19] performed two-phase flow simulation on twin-screw pump for 0 and 50% GVF. Significant flow separation was observed beyond bubble size of 0.12 mm for twin-screw pump operation. From the research it is evident that bubble size was the dominant factor in accurately modeling the two phase flow in different type of pumps.

1.4 Numerical Studies for Viscosity

Several researchers have conducted studies on the influences of viscosity on pump performance. Amaral, Estevam and Franca [20] researched the effects of viscosity to understand how overall performance of an ESP changes for working fluids with altered viscosity. They used water and glycerin as a working fluid and they changed the glycerin viscosity between the range of 60 cp and 1,020 cp by regulating the working fluid temperature. The viscosity of water remained same (1 cp) during experiments. A three-stage, semi-axial GN7000/540 Series type ESP was investigated in this work. Each stage consisted of 12 vane diffusers and 8 blade impellers. In Figure 25, selected zones for pressure measurements are numbered, where 1 is the diffuser inlet, 2 is the diffuser outlet/impeller inlet, and 3 is the impeller outlet/diffuser inlet of following stage.

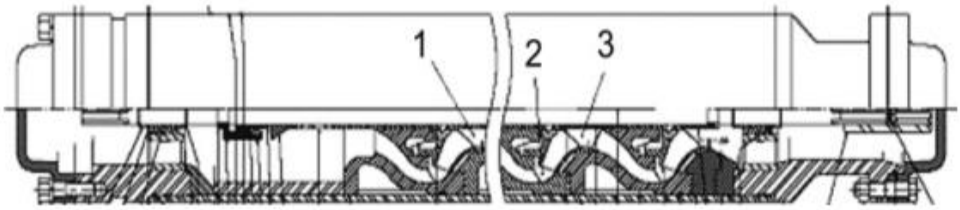

Figure 25 View of GN7000 [20]

For 1800 rpm, 2400 rpm, 3000 rpm and 3500 rpm nominal speed of impeller, the authors repeated experiments for different viscosity fluids and obtained head curves. Head curves for fluids with different viscosities at 3500 rpm rotation speed are presented in Figure 26. The single cross on each curve in the figure represents the best efficiency points.

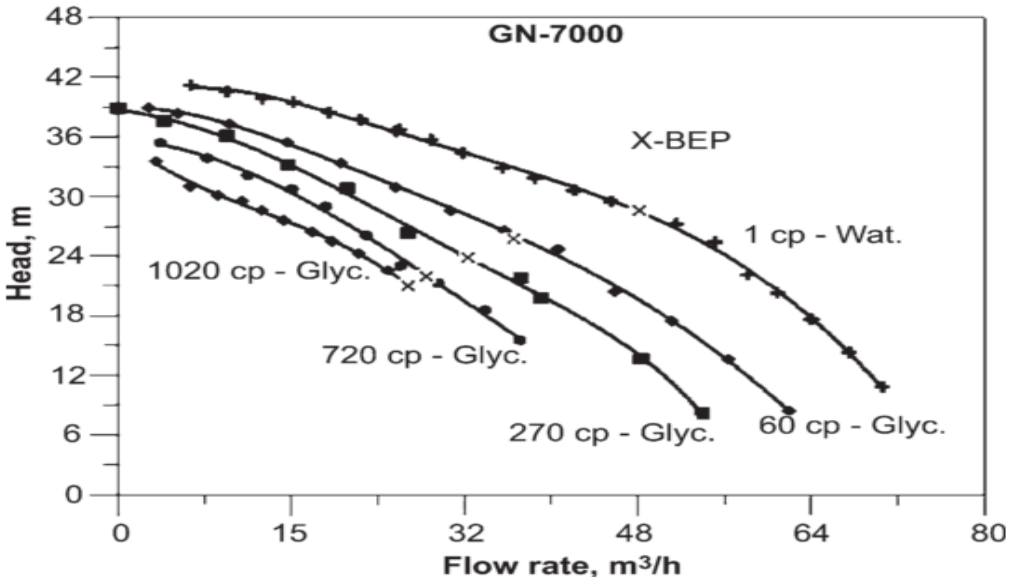

Figure 26 Head Curve Changing by Viscosity [20]

Through this experiment, a noticeable head decrease with increasing viscosity was monitored. The authors pointed out that changing viscosity from 1cp to 60 cp effects the pump performance more than changing viscosity from 270 cp to 720 cp. Obtained heads and the BEP of the pump changes with respect to fluid viscosity. Thus, authors concluded that viscosity plays an important role on ESP pump performance.

Another work carried out by Sirino, Stel and Morales [21] was also focused on the effects of viscosity on ESP performance. By taking results of Amaral, Estevam[20] as a reference, researchers performed a numerical analysis of a single stage GN7000/540 Series type ESP. The entire stage of the ESP system consisted of a 7 vane diffuser and a 7 blade impeller. Entire stage is illustrated in Figure 27. General dimensions of entire stage are tabulated as Table 3.

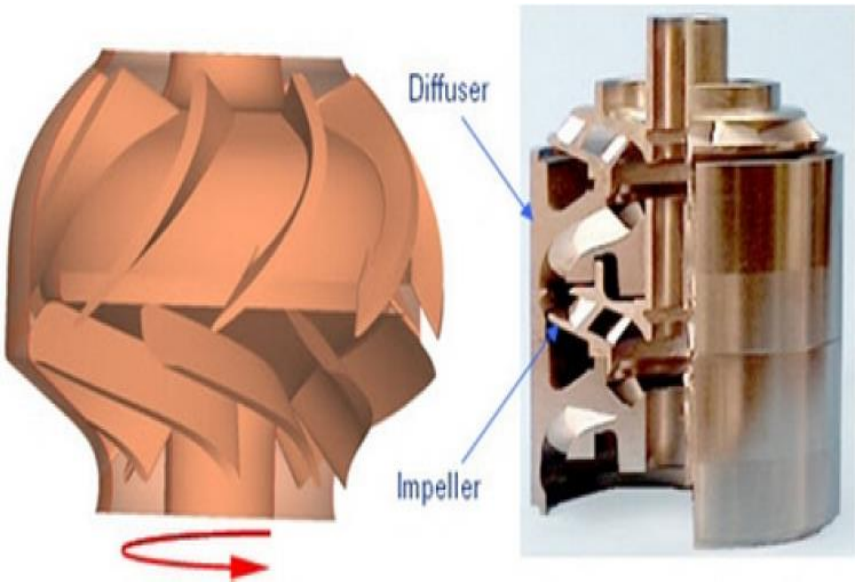

Figure 27 Vane Diffuser & 7 Blade Impeller [21]

Table 3 Dimensions of GN7000 [21]

Description	Impeller	Diffuser
Number of blades/vanes	7	7
Inlet inner diameter	25.4 mm	83 mm
Outlet inner diameter	83 mm	25.4 mm
Inlet outer diameter	65.2 mm	93.7 mm
Outlet outer diameter	93.7 mm	65.2 mm
Inlet blade height	17.3 mm	42 mm
Outlet blade height	15.7 mm	74 mm
Inlet blade thickness	2 mm	3 mm
Outlet blade thickness	3 mm	4 mm
Inlet blade angle	28°	25.5°
Outlet blade angle	36°	90°

For the numerical processes, the authors used the commercial program ANSYS CFX. They used a model of the ESP without balance holes by neglecting any sort of leakage on the stage. A pipe which includes both inlet and outlet of the entire system was inserted to the domain in order to enhance numerical calculations and eliminate uncertainties. The meshed domain and boundary conditions of pump is represented in Figure 28.

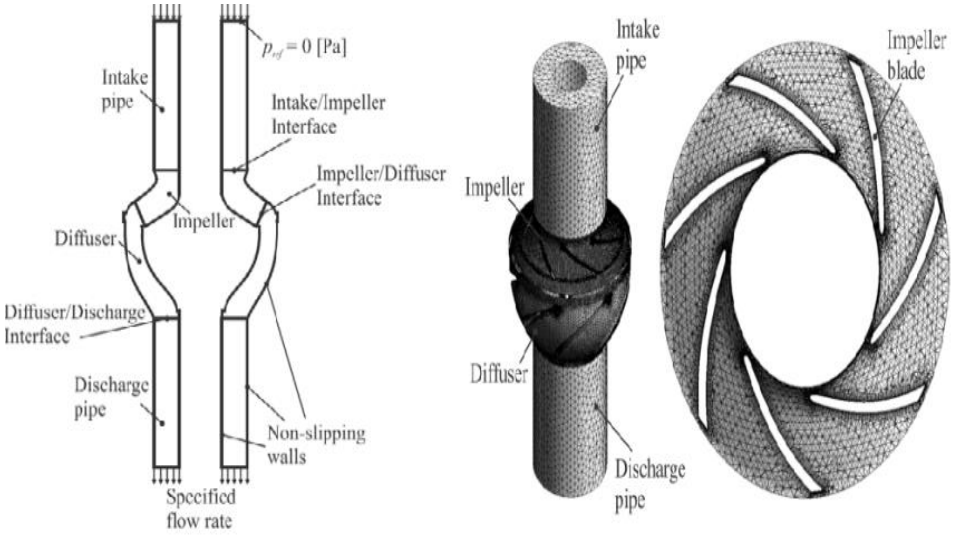

Figure 28 Boundary Conditions and Mesh Domain [21]

Using around 2.3 million elements, tetrahedral non-structured mesh was utilized for the entire stage. At some crucial zones such as impeller blade surfaces, prismatic elements are also used. Different case scenarios were investigated. As Amaral, Estevam and Franca [20] did, the researchers considered different operating fluids with changing viscosity from 1 cP to 1020 cP. They calculated Reynolds numbers less than 1000 when the minimum value of fluid viscosity was 270 cP. Therefore, between 270cP-1020 cP range, the authors treated the cases as a laminar flow and did not apply a turbulence model. However, for 1 and 60 cP fluid viscosities, they used the Shear Stress Transport turbulence model when the Reynolds number was greater than 2000. For 3500 rpm impeller rotation speed, they obtained single stage head curves. Figure 29 shows the comparison between experimental and numerical results at various rotation speeds and when the fluid viscosity was 1 cP.

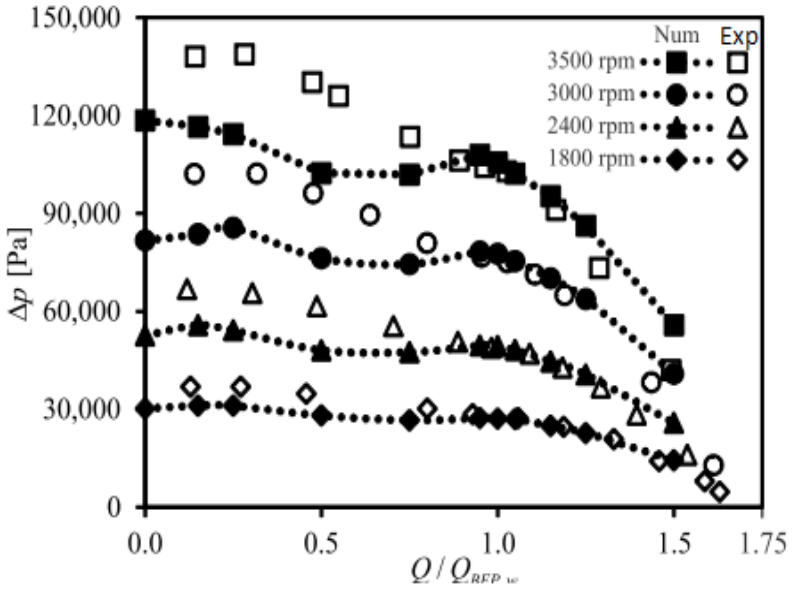

Figure 29 Comparison of Single Stage Pressure Change Between Numerical and Experimental Results for 1cP [21]

In general, comparison of the pressure difference between experimental and numerical results showed a good agreement for all operating fluids regardless of their viscosity.

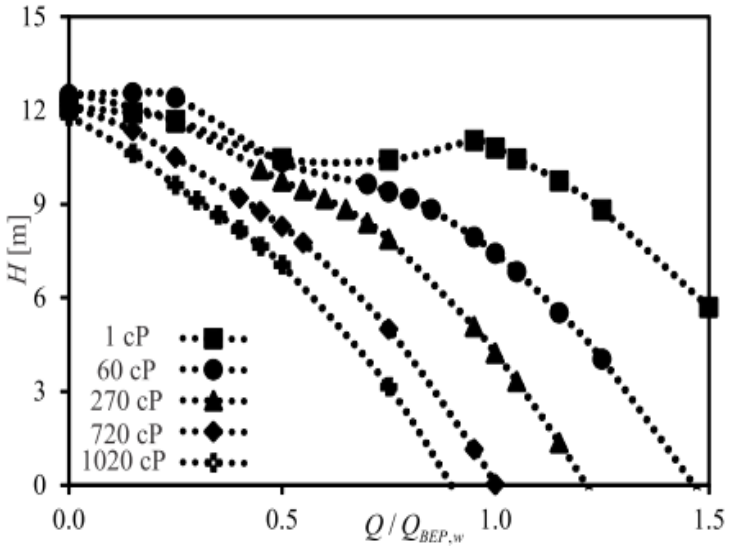

Figure 30 Head Curves for Single Stage at 3500 rpm [21]

From Figure 30, the tendency of head curves with respect to different fluid viscosities also had a good agreement with experimental data. By this study, researchers demonstrated that CFD is a powerful tool to visualize the effect of viscosity on pump performance.

To observe the effects of liquid viscosity on erosion damage, Okita, Zhang, McLaury and Shirazi [22] conducted a detailed study which covers both experimental and numerical tests. They developed an erosion formula at Erosion/Corrosion Research Center (E/CRC) using a nozzle system. The target material of this study was aluminum 6061-T1. As seen in Figure 31, they divided their study into 5 main steps.

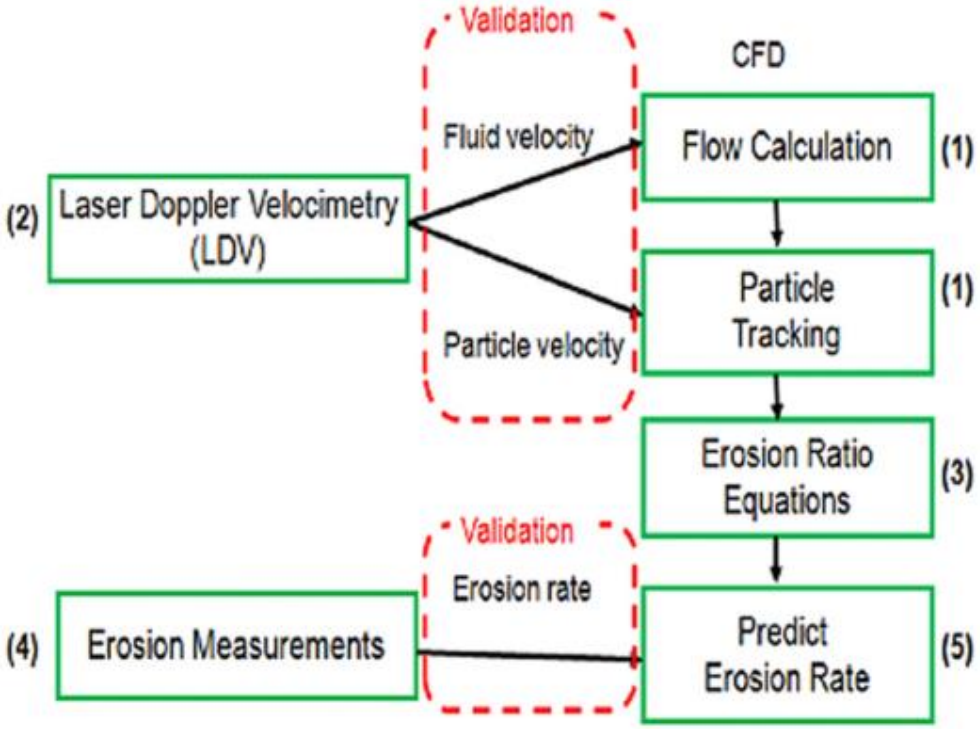

Figure 31 Steps of Erosion Prediction Process [22]

During the first step, the authors performed flow speed calculations and particle tracking using a CFD based computer program. They obtained the general data of flow field, such as pressure, fluid and particle velocities. In the second step, the researchers measured real particle and fluid velocities with different viscosities as the confirmation of the previous step. Sufficient erosion information for aluminum 6061-T6 was presented in the third step. In the fourth step, obtained data from the third step was recalculated based on if the target material was submerged in fluid with various viscosities. Lastly, erosion rates were predicted with the light of information obtained by earlier steps. To find erosion ratio correlation for the target material Al 6061- T6, other erosion equations developed by previous researchers were considered by E/CRC.

$$ER\left(\frac{kg-material\ loss}{kg-sand}\right) = F_s.C.(BH)^{-0.59}.V^n.F(\theta) \quad (2)$$

$$BH = \frac{(\mathrm{H_v} + 0.1023)}{0.0108} \quad (3)$$

$$F(\theta) = \frac{1}{f}.\sin(\theta)^{n_1}.\left(1 + H_v^{n_3}(1 - sin\theta)\right)^{n_2} \quad (4)$$

In equations 2, 3, and 4 above, ER refers the ratio of erosion, F_s is the sharpness factor (changes between 0.2 and 1), C and n are experimental coefficients, BH is the Brinell Hardness, V is the particle impact velocity, F(θ) is the impact angle function, and H_v is the Vicker's Hardness.

Equation 2 is the formula to predict erosion rate on carbon steel developed by McLaury [23], and Equation 4 is a reformed version of impact angle equation, which was originally generated by Oka, Okamura and Yoshida [24] as,

$$ER = K.(H_v)^{k_1}.\left(\frac{V}{V'}\right)^{k_2}.\left(\frac{D}{D'}\right)^{k_3}.\rho.F(\theta) \quad (5)$$

$$F(\theta) = (sin\theta)^{n_1}.\left(1 + H_v(1 - sin\theta)\right)^{n_2} \quad (6)$$

Where $V'$and D' are the reference values obtained from experiments, $F(\theta)$ is the function of impact angle, ρ is density of target material, and K, $k_1, k_2,$ and k_3 are the coefficients for hardness of material. Sufficient data for constants used in the studies is given in Table 4.

Table 4 Coefficients for Erosion Equations [22]

Oka's Equation		Erosion/Corrosion Research Center		
Variable particle size		150 μm particle size		300 μm particle size
H_v(Gpa)	1.12	H_v(Gpa)	1.12	1.12
k	65	F_s	0.50	1.00
k1	-0.12	f	5.27	2.19
k2	$2.3(H_v)^{0.038}$	n1	0.59	0.50
k3	0.19	n2	3.60	2.50
n1	$0.71(H_v)^{0.14}$	n3	2.50	0.50
n2	$2.4(H_v)^{-0.94}$	C	1.50E-07	3.28E-07

Equations (2), (3), and (4) were used to predict the erosion. Various particle sizes(20,150,and 300 μm) and carrier fluids with different viscosities (1, 10 25, and 50 cP) were selected for the tests. The erosion rate for the experimental test was calculated by

$$ER_{mass}\left(\frac{kg}{kg}\right) = \frac{W_{before}(kg) - W_{after}(kg)}{\dot{m_{sand}}(\frac{kg}{s}).\, t_{test}(s)} \quad (7)$$

Where $\dot{m_{sand}}$ is the mass flow rate of sand, t_{test} is the time of testing, and W is the weight of target zone. The obtained erosion results by experiments are given in Table 5. Standard deviations are found by repeating the same test multiple times.

Table 5 Erosion Results by Experiments [22]

	300 µm		150 µm		20 µm
Viscosity(cP)	Value	Standard Deviation	Value	Standard Deviation	Value
1	3.21E-06	4.37E-07	1.46E-06	2.18E-07	9.78E-08
10	2.56E-06	8.12E-08	1.07E-06	9.21E-08	3.83E-08
25	2.69E-06	1.81E-08	7.03E-07	6.57E-08	2.30E-08
50	2.83E-06	4.04E-07	4.29E-07	2.39E-07	1.28E-08

Figure 32 shows the measured relation between erosion rate and the viscosity value of the carrier fluid for different particle sizes. It was noted that the 20 µm fluid particles were affected by the increased viscosity more than both the 150 and 300 µm particles.

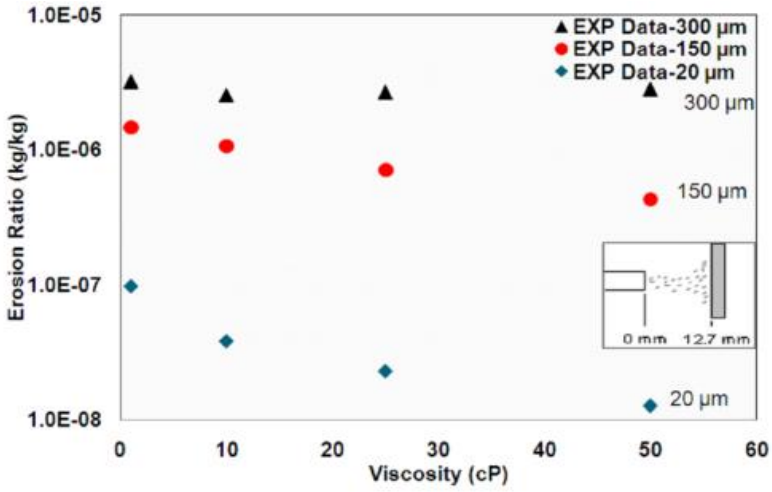

Figure 32 Erosion vs Viscosity [22]

Using air as a career fluid, for 13 m/s particle impact speed, the change of the erosion rate with respect to impact angle for 150 and 300 µm was obtained. Under these

conditions the differences between the E/CRC formula, Oka's formula, and the experimental results were compared in Figure 33.

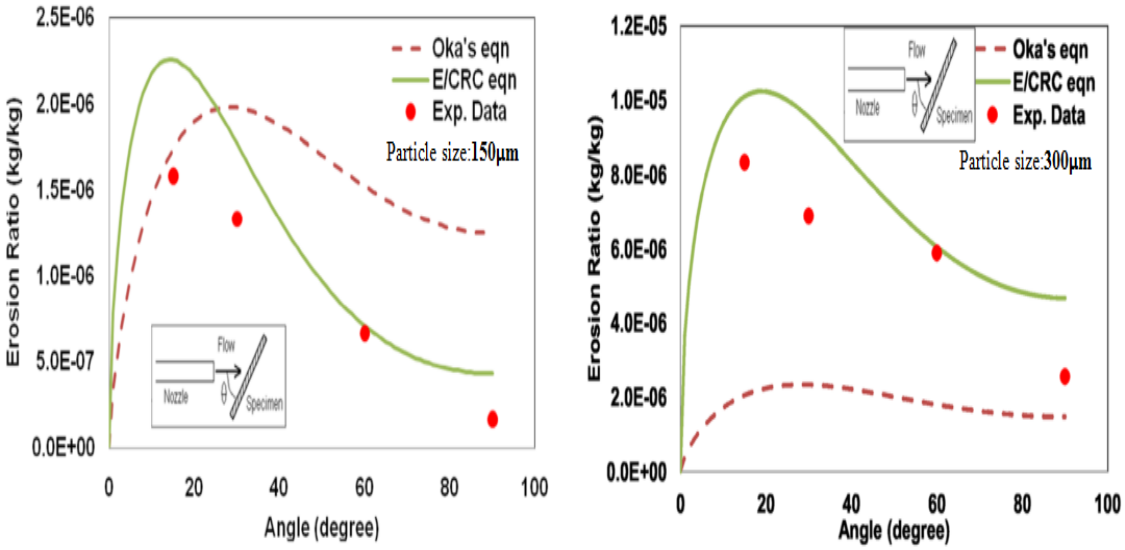

Figure 33 Erosion Ratio vs. Impact Angle for 150 and 300 μm, respectively [22]

To normalize the erosion rate, the authors divided the experimental erosion rate by an erosion rate at θ=15 degree due to nozzle's impact angle to the target zone.

$$ER_{normalized} = \frac{ER\left(\frac{kg}{kg}\right)}{ER_{\theta=15}\left(\frac{kg}{kg}\right)} \tag{8}$$

Comparison of normalized erosion rates obtained by CFD and experimental tests for aluminum 6061-T1 are presented as Figure 34.

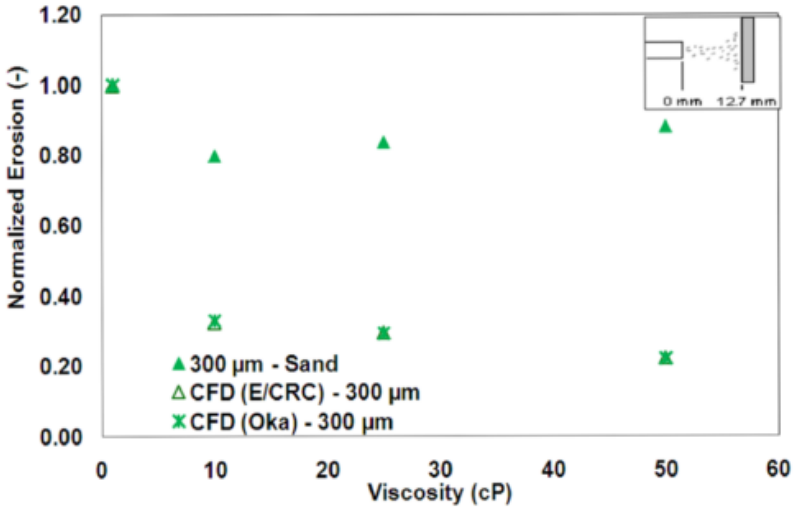

Figure 34 Experimental Data and Normalized Erosion Rate for 300 µm [22]

Both E/CRC and Oka CFD model have the same tendency for 300 µm particle size. Comparisons for 150 µm and 20 µm are presented in Figure 35.

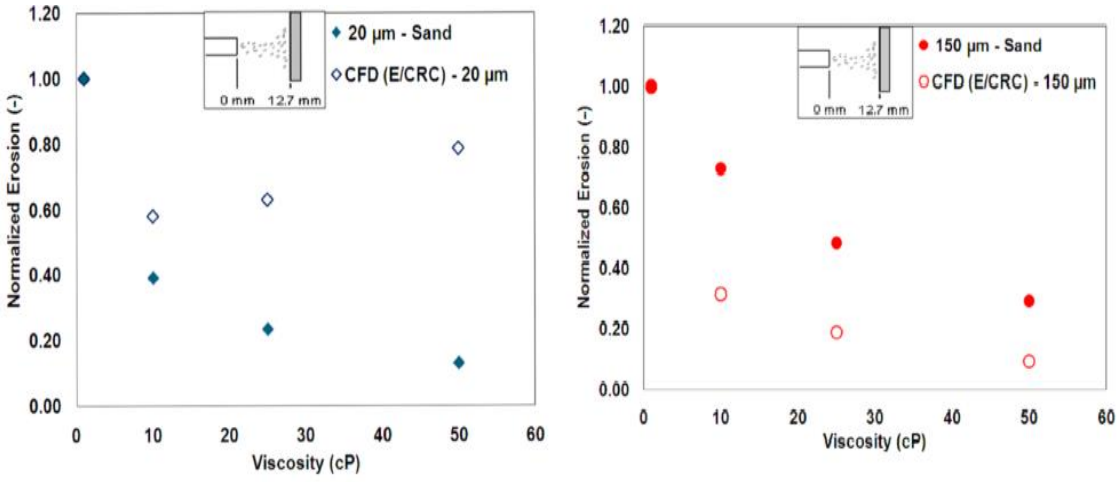

Figure 35 Experimental Erosion and Normalized Erosion Prediction for 20 and 150 µm Particles [22]

CFD results gave a good result especially for 150 μm particle size. Obtained erosion trend by CFD was similar to experiment results. This study shows that erosion rate on the target material can be predicted by a developed erosion formula.

1.4.1 ANSYS Erosion Module

Due to solid particles in the flow regime causing damage to the surface of working equipment, ANSYS Fluent developed an Erosion Module which helps to evaluate the effects of sand on erosion. The Erosion Module is based on a Discrete Phase Model (DPM).

In DPM, while primary fluid flow is calculated in an Eulerian methodology, discrete phase (particles, bubbles, etc.) are computed in a Lagrangian frame. Practically, discrete phase is applicable at lower fraction rates(less than 10-12%) to work with the Erosion Module. The module provides a good number of credited erosion models in the literature that were developed by researchers. It is possible to predict the location and magnitude of erosion of working equipment using this module[25].

2. OBJECTIVES

The main objective of this study is the CFD based erosion prediction of mixed flow ESP for different viscosity fluids. Flow analysis of the ESP for service with the sand mixtures of 1 cP, 5 cP, 20 cP, and 60 cP fluids are obtained in the Eulerian frame. Erosion rate on the impeller blades is visualized using the equation developed by Pirouzpanah [26] in the Turbomachinery Laboratory at Texas A&M University. In addition to the Eulerian approach, the simulation is carried using the ANSYS Erosion Module which applies Discrete Phase Module to predict erosion. Comparison of the developed model and ANSYS Erosion Module is obtained.

Prior testing at Turbomachinery Laboratory showed that the presence of air has a profound effect on erosive wear of ESP systems. The second objective of this study is to evaluate the effect of gas presence on erosion wear of ESP system using three phase CFD simulations. For this simulation, two phase water/air flow was modelled to evaluate the effect of bubble size on flow separation and pump performance. Then, three phase flow (water-sand-air) at 15 % GVF was modelled to observe the effect of air on erosion.

In order to reduce complexity, only a single stage of a multistage pump is considered to reduce the computer requirement for the CFD simulations. For numerical analysis, a commercial program ANSYS Fluent is used. For single phase flow simulations, the validation of the CFD model is obtained through comparison with experimental data from previous studies performed in Turbomachinery Laboratory.

After validation is completed, complex experiments can be replaced by CFD simulations resulting in time and cost savings since the CFD model can be used in different working conditions.

3. PROCEDURES

3.1 Experimental and Numerical Results from Previous Studies

Experimental data for 3 stages of a mixed flow type ESP which rotates 3600 rpm were obtained by previous studies at Texas A&M University, Turbomachinery Laboratory. Impeller and diffuser sections of a single stage are presented in Figure 36.

Figure 36 Impeller Suction and Diffuser Discharge Sections, respectively [27]

Dimension specifications information of the pump which are obtained from the previous experimental studies performed in Turbomachinery Laboratory are given in Table 6.

Table 6 Mixed Flow ESP Dimensions

Description	**Impeller**	**Diffuser**
Number of blades/vanes	5	7
Inlet inner diameter	48.2 mm	183 mm
Outlet inner diameter	183 mm	48.2 mm
Inlet outer diameter	116.5 mm	218.6 mm
Outlet outer diameter	218.6 mm	116.5 mm
Inlet blade height	35 mm	19.8 mm
Outlet blade height	24.8 mm	22.9 mm
Inlet blade thickness	4.8 mm	3.8 mm
Outlet blade thickness	2.1 mm	4.8 mm

The experimental program was divided into two steps. For the first step, an ESP was operated with pure water-sand two phase flow conditions for 117 hours. Then, the performance of pure water, sand and air (15% GVF) three phase flow was recorded an for additional 68 hours in the second step and performance curves were obtained for both cases. While volume flow at the inlet was 1100 GPM for two phase flow, 1000 GPM was used for the three phase case.

After the first 117 hours, when pure water - sand mixture was used as the working fluid, pressure rise between inlet and outlet of the three stages pump system was measured around 200 psi for 1100 GPM volumetric flow rate at the inlet given as Figure 37.

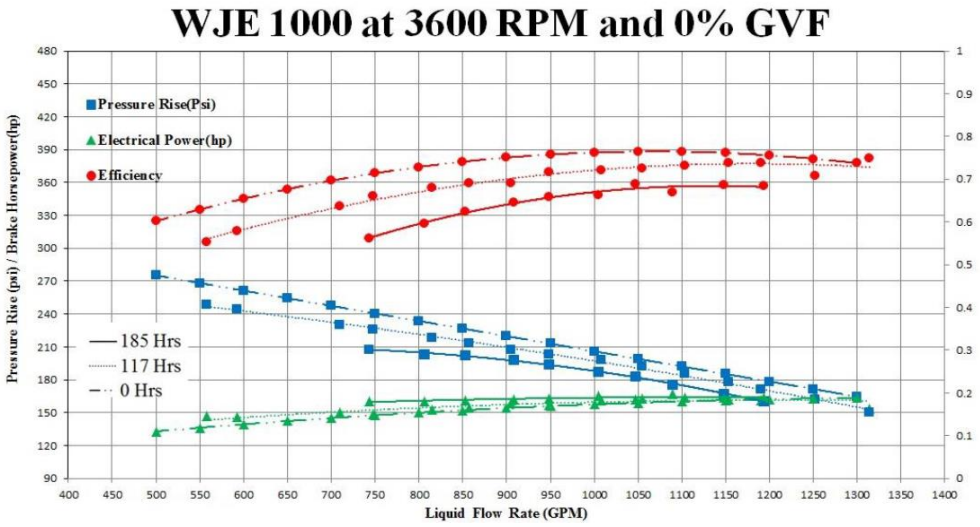

Figure 37 Pump Performance Curve of Three-Stage ESP for 0% GVF [28]

In another experiment which was performed again in Texas A&M University, Turbomachinery Laboratory, single stage pump performance with water- sand mixture is illustrated in Figure 38.

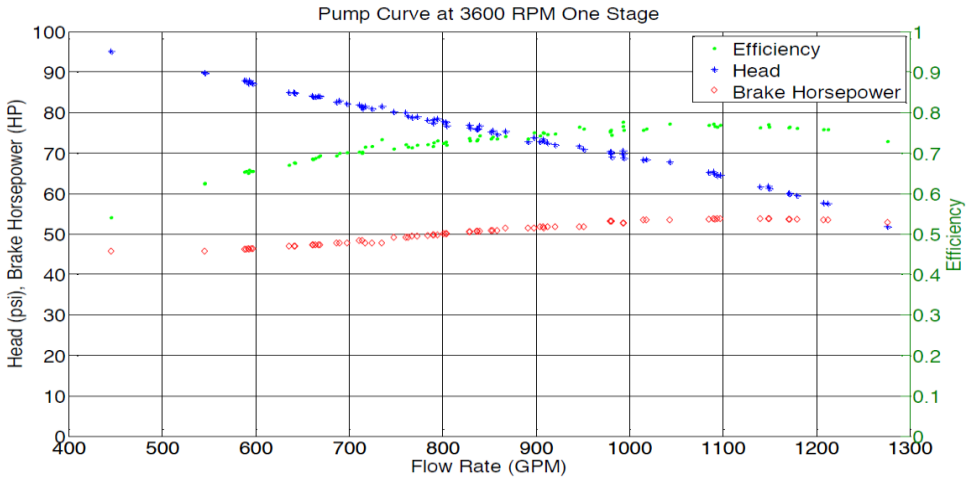

Figure 38 Pump Performance Curve of Single Stage [27]

After 185 hours, when air was considered as a part of the working fluid, the attained pressure rise on the three-stage ESP was around 125 psi for 1000 GPM total flow rate at the inlet and 15% GVF. Figure 39 shows the pump performance at 15 % GVF.

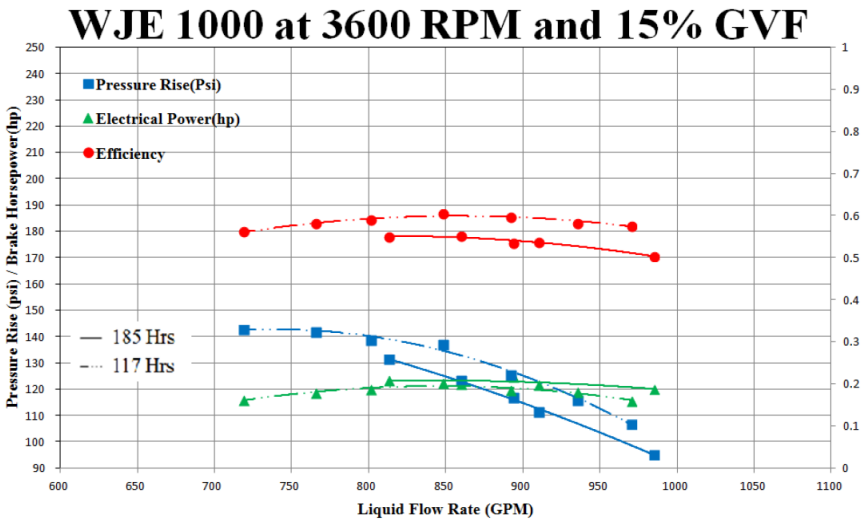

Figure 39 Pump Performance Curve of Three-Stage ESP for 15% GVF [28]

In addition to the experiments, computational studies were also performed. For the BEP of the pump at the rotation speed of 3600 rpm, the CFD simulations of pure water and water-sand mixture (2 gr/lit concentration) were modeled by Pirouzpanah [26]. For single phase flow, the comparison of generated pressure for a single stage between experimental and numerical results is represented in Table 7. Very small levels of difference are observed. For the first stage, five balance holes were used to reduce the axial force loaded on the impeller. Balance holes were periodically placed on the impeller hub surface. Assuming a discharge coefficient of 0.6, the leakage of mass flow

rate through the balance holes was predicted as 5% of the total mass flow rate at the inlet.

Table 7 Experimental and Numerical Stage Pressure Rise Comparison for Single Phase Flow, 1100 GPM-3600 rpm [26]

Method	**Pressure Generation per Stage(psi)**
Experimental	65
CFD-1st Stage	66.7
CFD-2nd Stage	65.1

A study carried out by Krüger, Martin and Dupont [29] investigated the wear erosion on pump impellers. A sand mixture of fluid was simulated. Key parameters of the discrete phase (sand) and important flow conditions which generate erosion are listed as:

- Impingement angle
- Particle(sand) concentration
- Particle size and shape
- Hardness of the particle
- Turbulence in flow zone
- Secondary flow and vortices
- Velocity of the flow

Based on these parameters, a new erosion model to predict the erosion rate was developed by Pirouzpanah [26]. The relation between the erosion factor and turbulence kinetic energy, k_w, was obtained.

ESP erosion rates were obtained for the two-stage of ESP after developing the new model. The obtained erosion rates for the water-sand mixture were visualized as shown in Figure 40 and Figure 41.

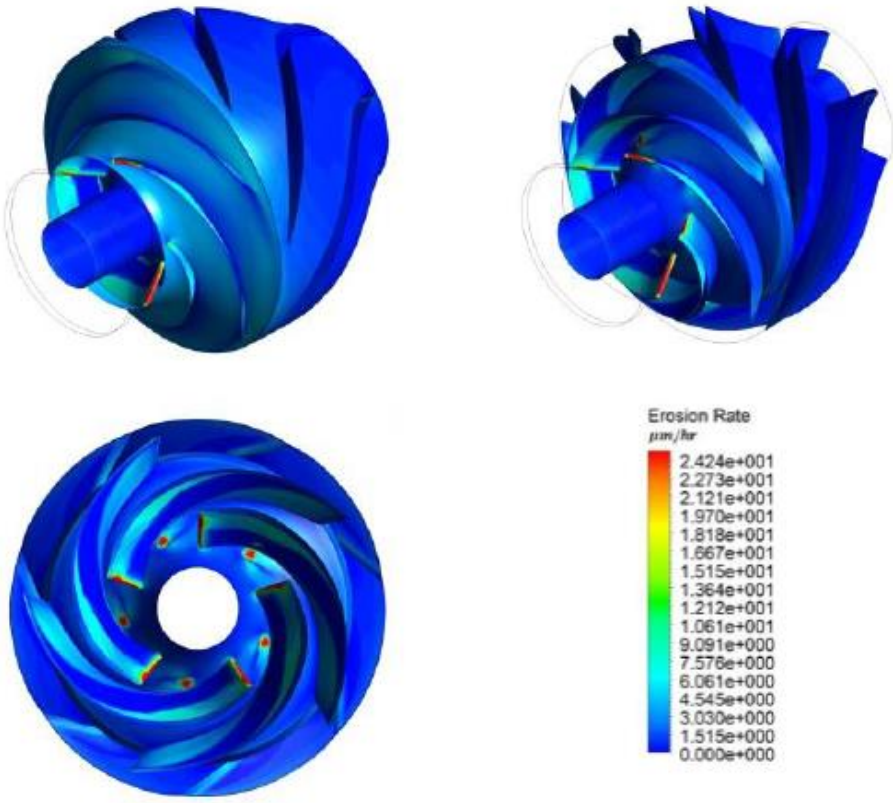

Figure 40 Erosion Rate Visualization with Developed Erosion Model [26]

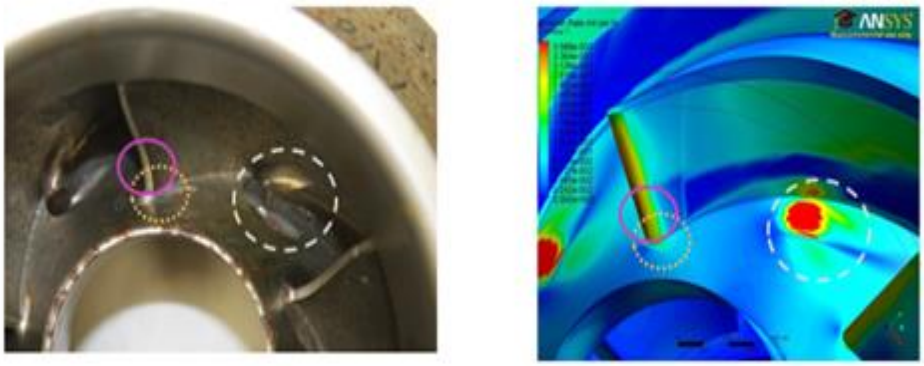

Figure 41 Comparison of Experimentally Eroded Locations and Developed Model [26]

This model showed that the effect of turbulence kinetic energy is an important factor for computing erosion rate.

In another study, using CFD, ESP efficiency curves for different viscosity fluids were obtained and tabulated in Figure 42 by Yin [30].

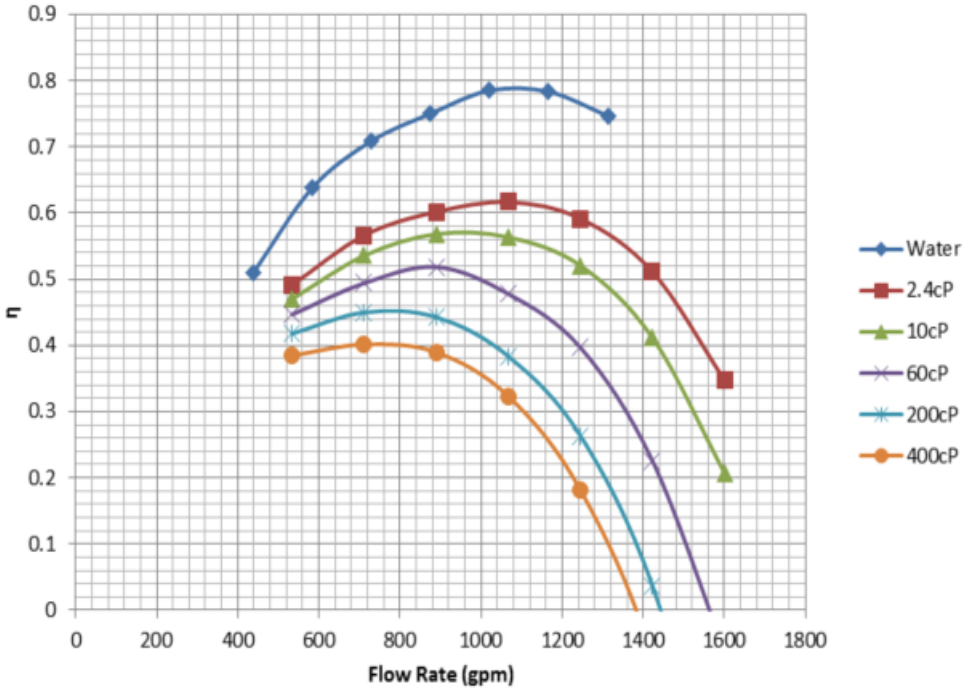

Figure 42 ESP Efficiency Curves for Various Viscosity Working Fluids [30]

3.2 Numerical Analysis

For the simulation part, due to saving time and reducing the number of iterations, only a single stage of ESP including balance holes is considered. The geometry of the mixed flow pump is given as Figure 43. After applying various mesh structures, the domain with structured hexagonal mesh is selected for computational analysis. CFD software ANSYS Fluent is used for simulations. Computers with different capacities are used to model the CFD simulations of the 7-vane diffuser and 5-blade impeller pump.

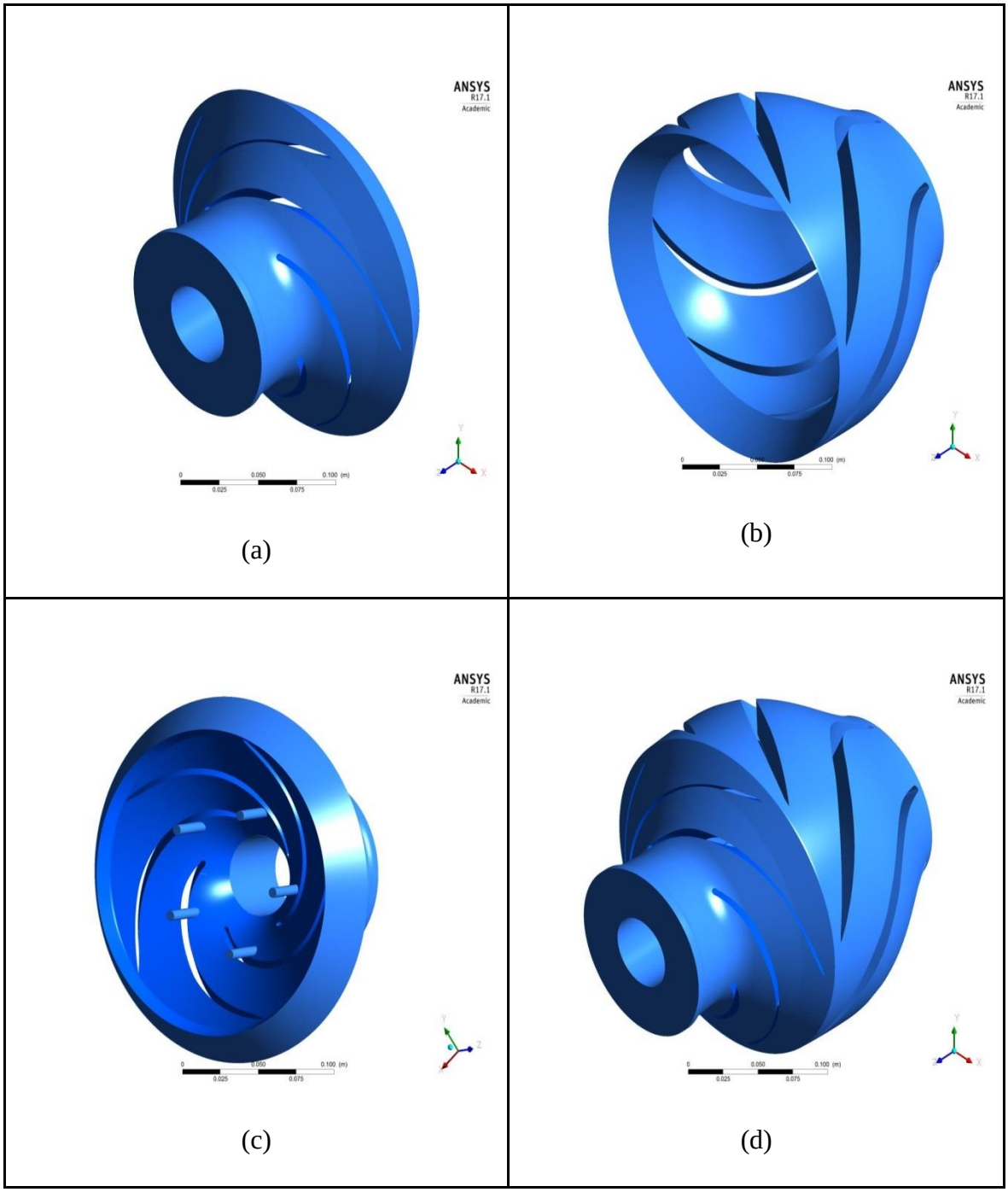

Figure 43 The Views of Impeller (a), Diffuser (b), Impeller Hub with Balance Holes (c), and Entire Stage (d)

The entire domain is divided into 4 main cell zones which are named as:

- Stage Inlet
- Impeller
- Balance Holes
- Diffuser

After named selections were done, the entire geometry was exported for meshing processes. Mesh statistics are presented in Table 8. The mesh domain used for the computational analysis is presented in Figure 44.

Table 8 Mesh Statistics

Domain	**Nodes**	**Elements**
Diffuser	2,714,631	2,591,325
Impeller	3,148,740	3,031,500
Balance Holes	22,155	20,000
Inlet	899,640	857,500
All Domains	6,785,166	6,500,325

Figure 44 Meshed Domain

CFD analysis is processed by using ANSYS Fluent. For all cases, simulations were carried out on the pump for 3600 rpm and various inlet mass flows with respect to BEPs. These flow parameters are also consistent to previous studies performed in Turbomachinery Laboratory. The performance curves for the three stages of ESP which rotates at 3600 rpm is given in Figure 45.

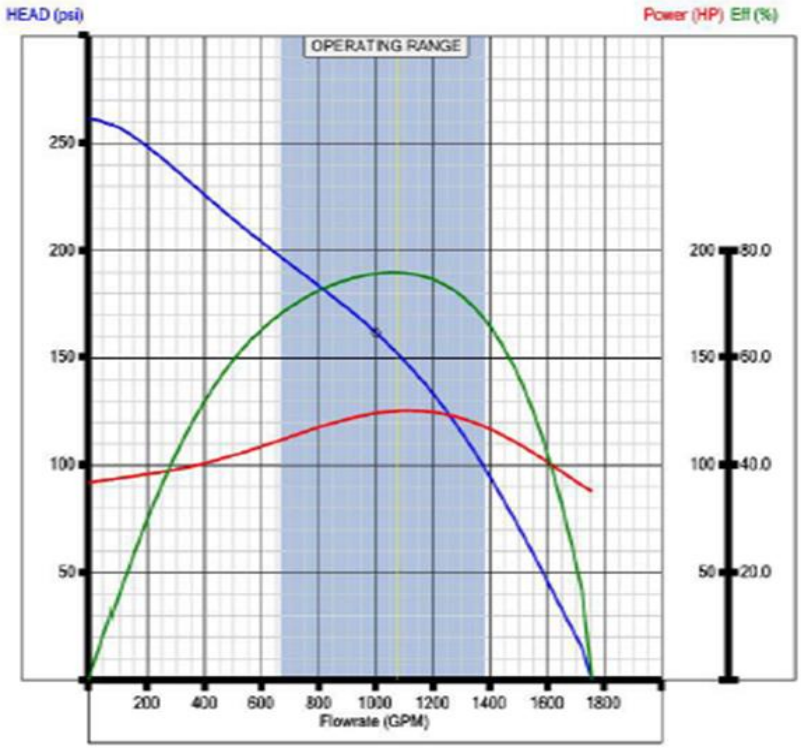

Figure 45 Catalog Specifications for Three Stage ESP - 3600 rpm [27]

Sand mixtures using various viscosity fluids are used in order to visualize the effect of viscosity on erosion of the ESP, especially on impeller blades. Using the developed model by Pirouzpanah [26], erosion rates were measured with the Eulerian approach. Simulations have been carried out for the BEP with respect to pump efficiency curves obtained by Yin [30] in previous studies. The test matrix of viscosity studies in the Eulerian frame is tabulated as Table 9.

Table 9 Test Matrix for Visualizing Effect of Viscosity on Erosion

Case	Fluid Viscosity(cP)	Impeller Speed(rpm)	Flow Rate at Stage Inlet(GPM)	Density (kg/m^3)
1	1	3600	1100	998
2	5	3600	1000	818
3	20	3600	910	818
4	60	3600	890	818

In CFD models, sand diameters are set to 150 μm, which is the same particle size used in the previous experiments. Since the real case scenario is time-dependent, transient analysis is performed in ANSYS Fluent to obtain accurate numerical results. Based on the literature review and previous studies, the standard k-ε model is selected for both single and multiphase simulations in order to model turbulence flow inside the ESP. For the k-ε model, the variable k refers to the turbulence kinetic energy, and ε refers to the turbulent dissipation rate which determines the magnitude of the turbulence. The standard k-ε model is a well-known model which is applicable for complicated turbulent flows.

After the working fluids and particles are created, cell zone conditions are set. Mesh motion is activated for the impeller and its boundaries while the entire diffuser zone is stationary.

In addition to the Eulerian approach, ANSYS Fluent Erosion Module, which is based on Discrete Phase Model (DPM), is used to visualize erosion rate in the Lagrangian frame. One cP (water) fluid-sand mixture is considered for DPM. Flow conditions are set to the same values which were used in the Eulerian approach. The

impact of erosion is visualized. After computational analyses are converged, results are transferred to CFD-Post.

4. RESULTS

4.1 Pump Performance

Pressure rise comparison is one the most important parameters for case validation. Pressure rise of the one stage ESP for pure water is given as 64 psi in the catalog performance specifications. When the BEP is considered, the obtained head for pure water by CFD simulation is 65.6 psi which shows a good consistency with the catalog performance curve. The pressure distribution of the single stage ESP is illustrated in Figure 46.

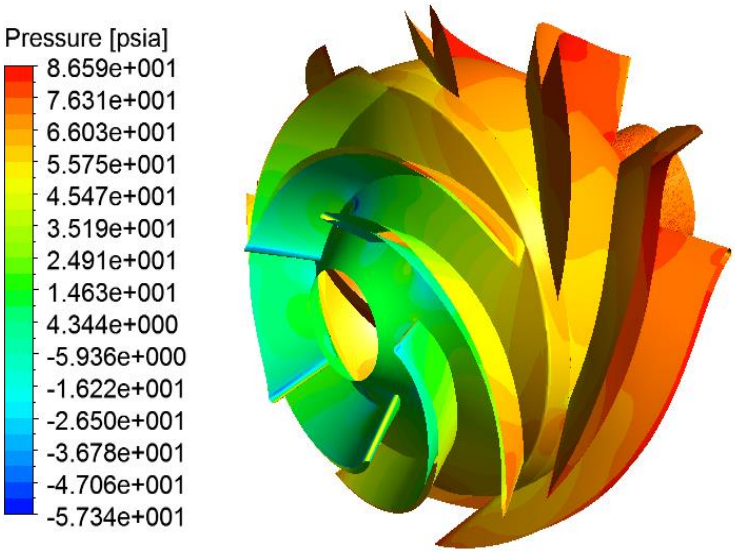

Figure 46 Pressure Contours of Single Stage ESP with the Service of Pure Water

Based on simulation results, the obtained heads from the single stage of the ESP for the mixture of sand and various fluid viscosities is tabulated in Table 10. Again, simulations are modelled at the BEPs for each case.

Table 10 Obtained Head of One Stage ESP

Viscosity (cP)	1	5	20	60
Pressure Rise (psig)	65.1	56.7	56.3	54.7

4.2 Flow Analysis

A commercial software CFD-post is used to analyze the flow field inside the pump. In order to have a better understanding of the flow field, the streamlines on the impeller and diffuser hubs are visualized. All shroud surfaces are set as hidden.

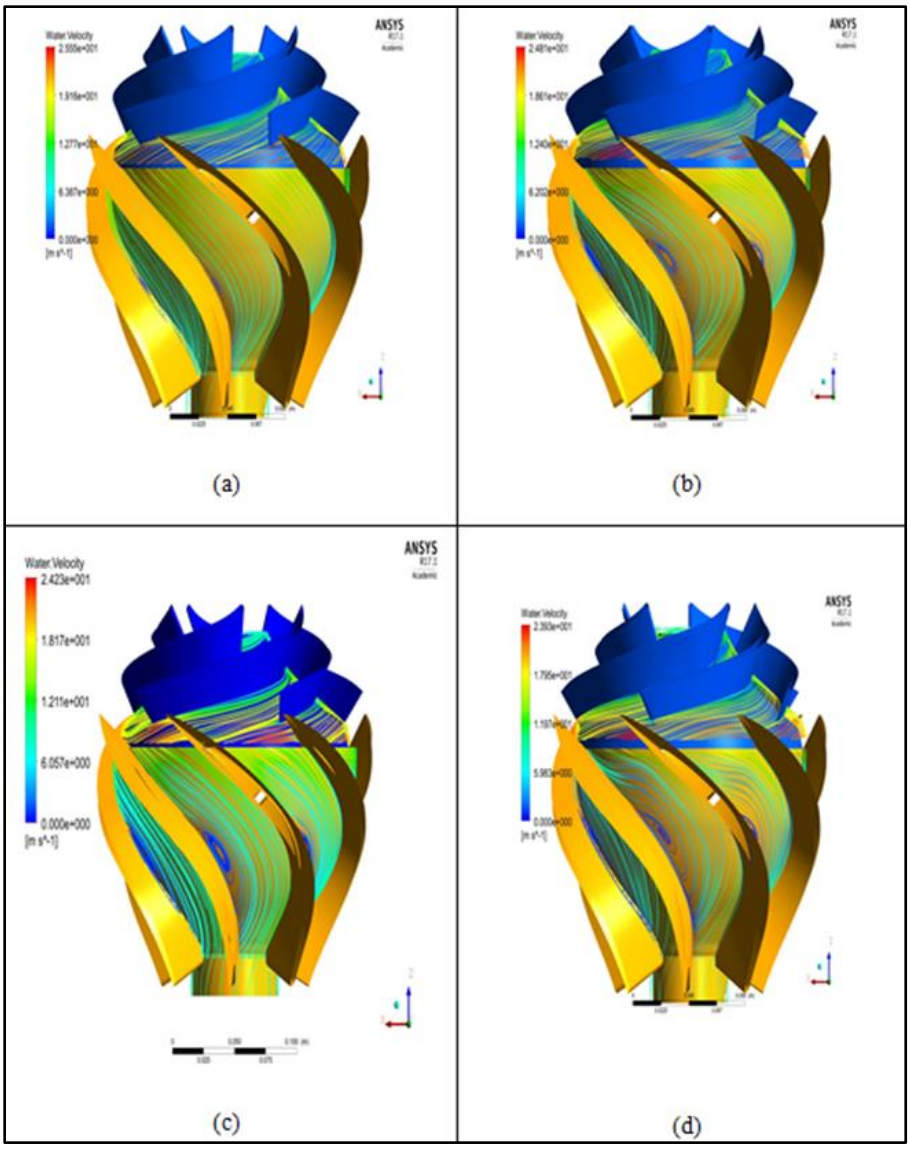

Figure 47 Streamlines in the Entire Stage at BEP for 1 cP (a), 5cP (b), 20 cP (c), and 60 cP (d) Fluids

Figure 47 illustrates the overall local water velocity streamlines inside the entire stage for various viscosities. For the same operating fluids, the recirculation regions will increase at the lower mass flow rates.

The recirculation zone on the diffuser hub surface is the largest for 60 cP fluid-

sand mixture when it is compared to others. Again, no change is visualized on the impeller hub surface. Since the flow fields are visualized for BEPs, altered recirculation zones are obtained with respect to different mass flow rates.

4.3 Erosion Visualization - Eulerian Approach

Simulating by the Eulerian approach is one of the most common methods in CFD analysis. The main properties of the Eulerian approach for multiphase flow simulation are:

- It treats dispersed phase as a continuum. All phases are considered as interpenetrating continuum.
- It is a result of solving and averaging Navier-Stokes equations for both primary and dispersed phase. A determined set of conservation equations for each phase forms the result
- It allows for mixing and separation of phases.

In the Eulerian approach, equations developed by Pirouzpanah [26] are used for visualizing erosion. Erosion model correlations were proposed with following equations:

$$EF = (\alpha_s)^{0.08} \left(\frac{V_s}{\overline{V_{s_0}}}\right)^{0.07} \left(\frac{k_w}{\overline{k_{w_0}}}\right)^{1.25} \quad (9)$$

$$ER\ (\mu m/hr) = A.EF^2 + B.EF \quad (10)$$

Where *A= 0.0163* and *B=0.8774* are empirical values, EF is the erosion factor (-), α_s is the sand concentration, V_s is the near wall sand velocity ($\frac{m}{s}$), $\overline{V_{s_0}}$ is reference

sand velocity (1 $\frac{m}{s}$), k_w is turbulent kinetic energy($\frac{m^2}{s^2}$), $\overline{k_{w_0}}$ is reference turbulent kinetic energy(1 $\frac{m^2}{s^2}$), and ER is erosion rate($\frac{\mu m}{hr}$).

The erosion rate visualizations are focused on the impeller since the erosion predominantly occurred on the impeller blades in experiments. Equation (9) and Equation (10) show that water turbulent kinetic energy (TKE) is an important parameter to predict erosion rate. In order to investigate the relation between the TKE and erosion rate, visualization of the TKE is obtained for the impeller blade surfaces.

4.3.1 Turbulent Kinetic Energy Visualization at the Impeller Blades

Using CFD Post, TKE distributions for the sand mixtures of operating fluids which have 1 cP,5 cP and 60 cP viscosity values are visualized. Figure 50 shows the TKE distribution for three different viscosity fluids and sand mixtures. The legend at the upper left corner shows the local range of TKE. The scale of the legend is set same for all cases to make comparison consistent. Figure 48 illustrates the TKE variation for 1, 5, 20 and 60 cP fluids.

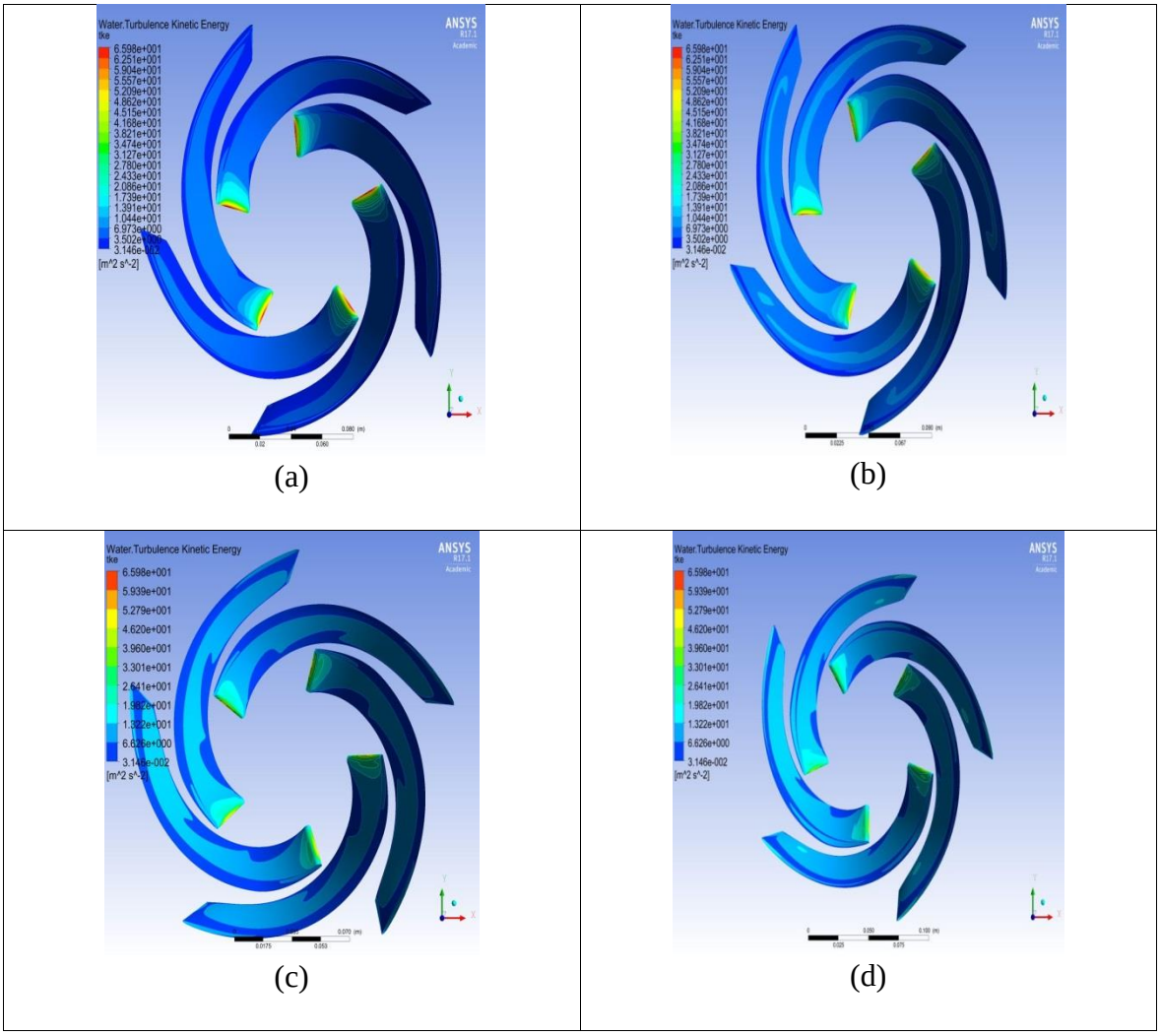

Figure 48 Turbulent Kinetic Energy on Impeller Blades for 1cP (a), 5 cP (b), 20 cP (c), and 60 cP (d) Fluid-Sand Mixture

For all cases, similar TKE variation trends are obtained. The value of the TKE attains its peak value at the leading edges of the impeller blades. Noticeably, using higher fluid viscosity caused to TKE density to decrease on the leading edges.

4.3.2 Erosion Visualization

After a simulation is converged, the solution is transferred to CFD Post. Then the erosion model developed by Pirouzpanah [26] is utilized. The erosion rate on the entire stage for the sand mixtures of 1 cP, 20 cP, and 60 cP viscosity fluids are obtained. The legends are set for the same range to make visualizations in the matching scale. Obtained erosion rates are illustrated in Figure 49. For all cases, developed erosion model by Pirouzpanah [26] showed a good consistency with obtained TKE distribution.

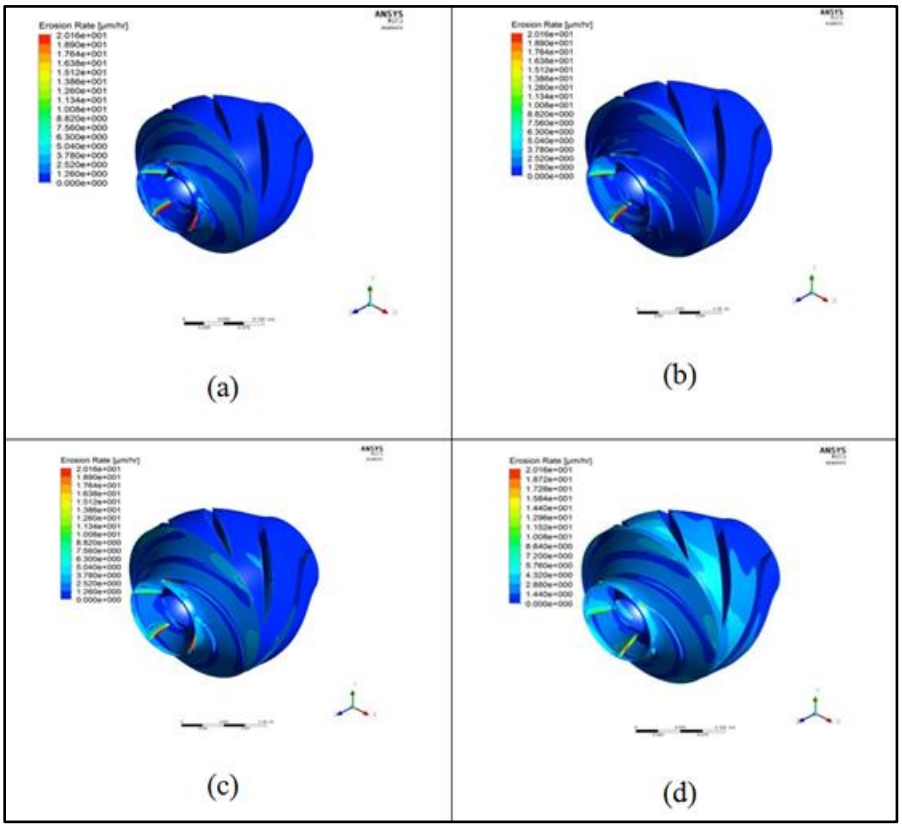

Figure 49 Isometric View of the Erosion Rate on the Entire Stage for 1 cP (a), 5 cP (b), 20 cP (c), and 60 cP (d) Fluids

As seen, the erosion rate attains its highest value at the leading edges where the maximum TKE value was observed. Noticeably, the erosion rate distribution obtained is similar to the TKE variation. Lower amounts of erosion rate are obtained when using higher viscosity fluid across the impeller blade leading edge. However, contrary to expectations, the erosion rate increased slightly with increase in viscosity across the diffuser. Different parameters such as increased localized recirculation, increased turbulence kinetic energy prediction due to higher dissipation or matter of fact accuracy of turbulence model may have affected this prediction. This observation needs to be validated using experimental testing. Since the impeller blades have the densest erosion, their comparison of the erosion rate on impeller blades is illustrated as Figure 50 in revised legend scale.

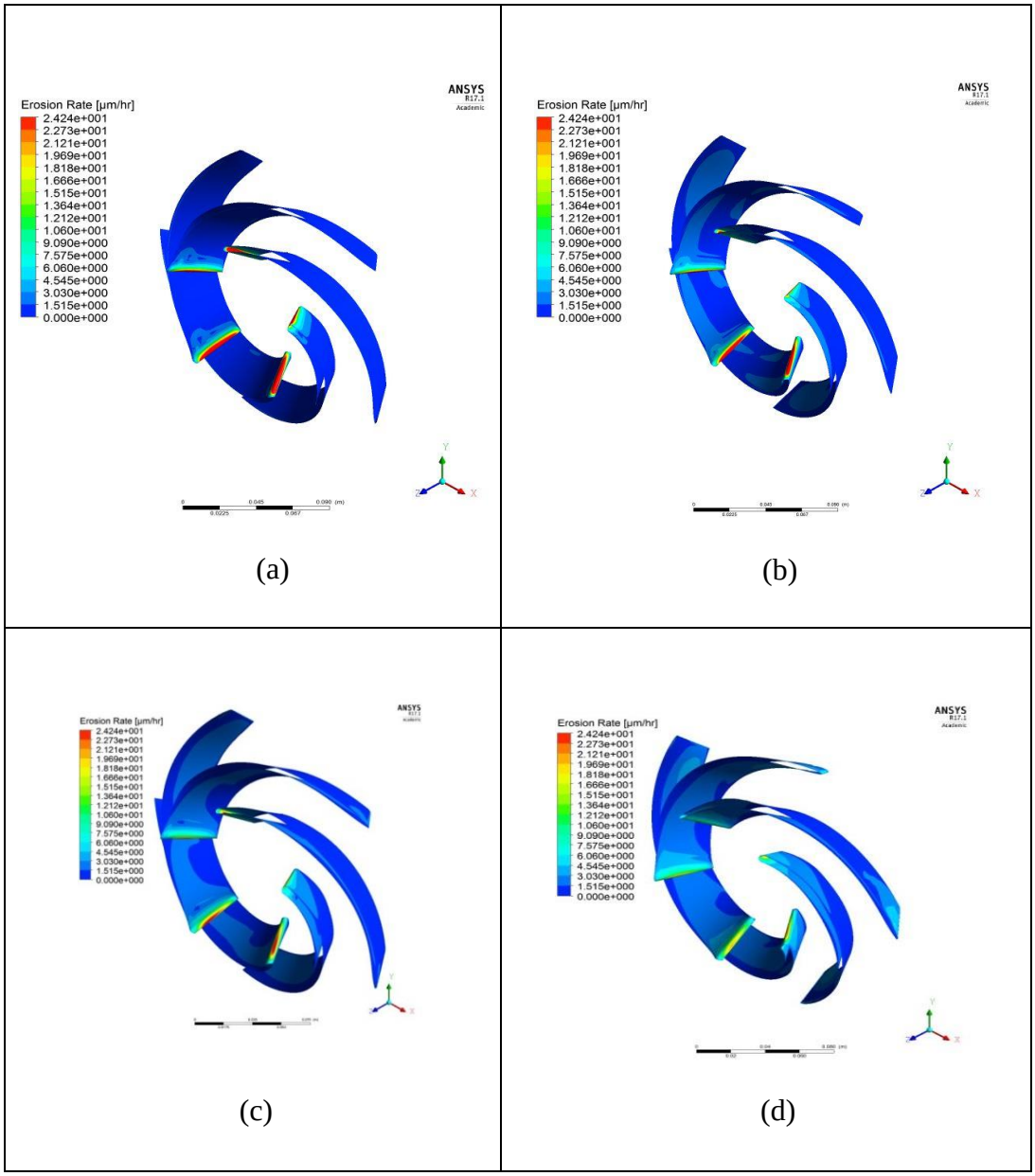

Figure 50 Isometric View of the Erosion Rate on the Impeller Blades for 1 cP (a), 5 cP (b), 20 cP (c), and 60 cP (d) Fluids

4.3.3 Erosion Visualization on the Impeller Hub

The range of legend is set the same for all operating fluids for consistency. For all cases, visualized erosion rates on the impeller hub are given in Figure 51. Relatively high levels of erosion are visualized for 1 cP fluid viscosity.

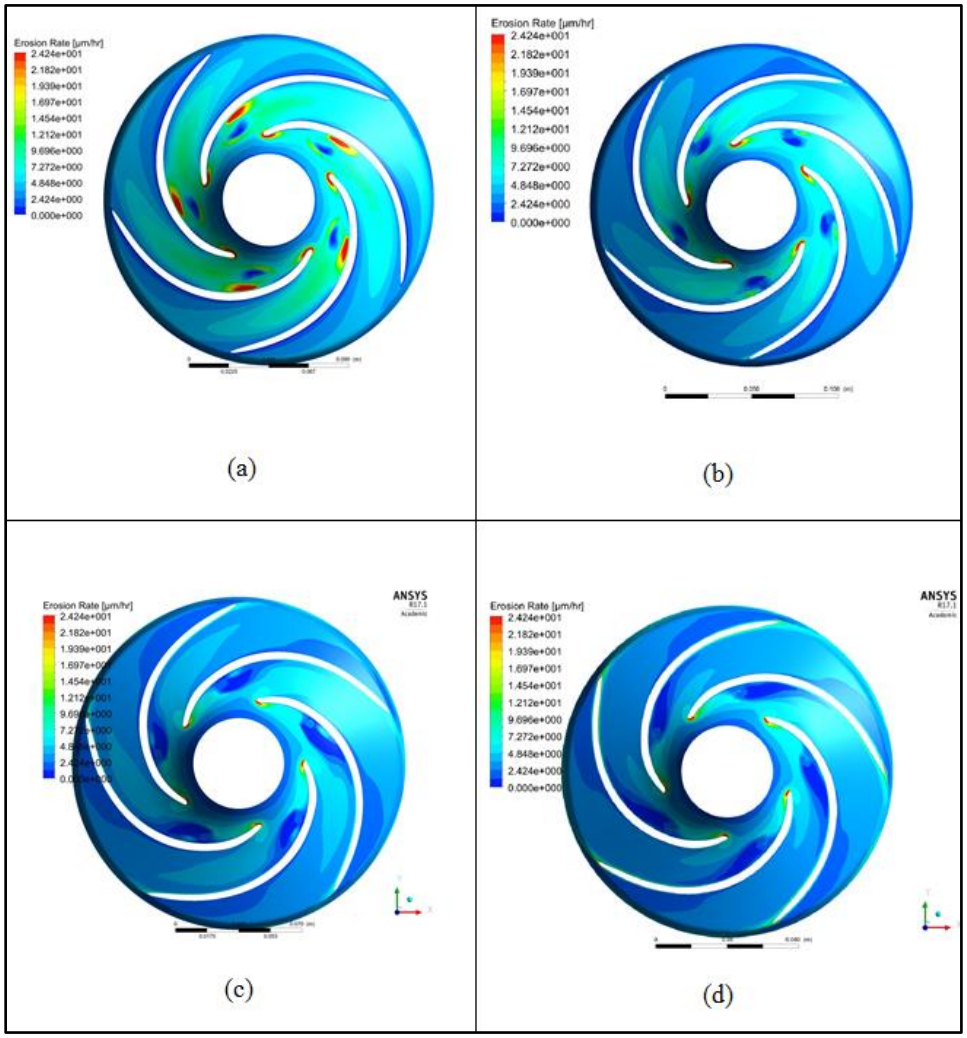

Figure 51 Erosion Rate on the Impeller Hub for 1 cP (a), 5 cP (b), 20 cP (c), and 60 cP (d) Fluid-Sand Mixtures

There is a significant decrease of the erosion rate as the viscosity is varied from 1 cP to 20cP. However, insignificant difference was observed between 20 and 60 cP. When the flow field of the 60 cP fluid was analyzed, a high value of dissipation and quite small values of y plus parameters are obtained. The flow regime is investigated by determining the Reynolds number which is defined by:

$$\mathrm{Re} = \frac{\rho \mathrm{V} \mathrm{D_h}}{\mu} \tag{11}$$

Where ρ is density of the operating fluid (kg/m^3), V is the velocity (m/s), D_h is hydraulic diameter (m), and μ is the viscosity (kg/m-s). The difference between the impeller inlet outer and inner diameters are used as the hydraulic diameter, D_h. The Reynolds number at the impeller inlet is calculated and tabulated in Table 11. Impeller inlet has a smaller diameter than the averaged diameter of the impeller hub which may cause a deviation of the calculation of the Reynolds number. However, due to the increase in viscosity value is quite higher than the hydraulic diameter change; the deviation because of the diameter difference is assumed negligible using Reynolds formula.

Table 11 Reynolds Numbers for 1 cP, 5cP, 20 cP and 60 cP Operating Fluids

Viscosity(cP)	Reynolds Number(-)
1	433,136
5	79,821
20	18,176
60	5,917

The relation between Reynolds number and flow regimes inside the pipe flow is given as [31]:

Flow is laminar for $0<Re<2100$

Flow is transient for $2100<Re<4000$

Flow is turbulent for $Re>4000$

Therefore, the flow inside of the ESP should be turbulent with respect to the flow zone limits. However, at 60 cP viscosity, the flow characteristics may not completely show the characteristics of turbulent flow due to the relatively low value of the Reynolds number. The flow may have both turbulent and transient zone properties for this particular viscosity value.

For all cases, standard k-Ɛ model is used to model turbulent flow. It is not clear that 60 cP fluid is totally in the turbulent region for the BEP. These are the main reasons which cause an error on visualizing erosion rate. As a matter of fact, it is hard to infer on the flow regime of centrifugal pump due to its complex geometry. The model developed by Pirouzpanah [26] provided good results for high Reynolds numbers.

As mentioned in the literature review, Okita, Zhang, McLaury and Shirazi [22] developed a model under the name of E/CRC in order to visualize the effect of viscosity

on erosion. Various fluid viscosities (1 cP, 10 cP, 25 cP, and 50 cP) were used as operating fluids. From experiments, they obtained a graphic of normalized erosion ratio vs. fluid viscosity for different particle diameters. The comparison of normalized erosion rates between the model developed by Pirouzpanah [26] and E/CRC is shown as Figure 52. Same particle diameters (150 μm) are used for the illustration.

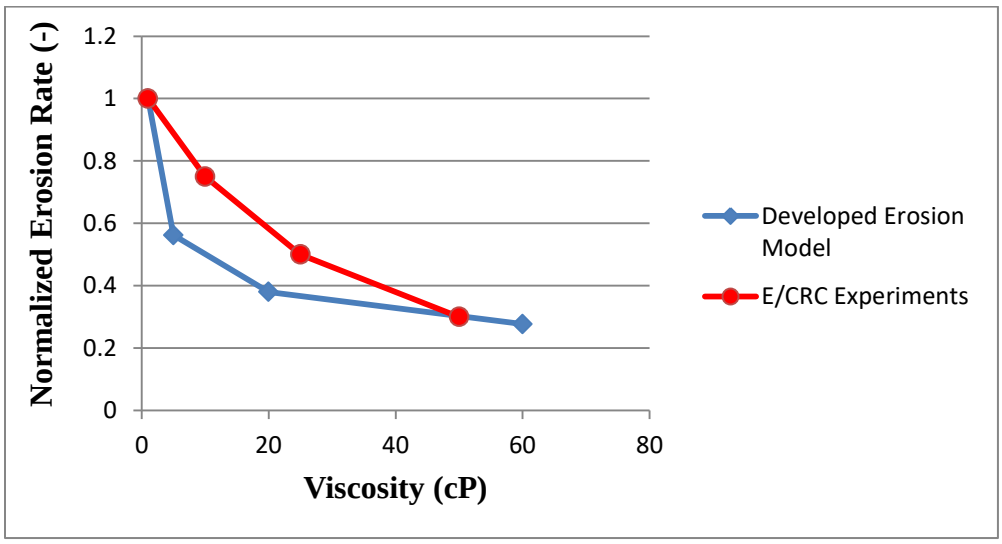

Figure 52 Normalized Erosion Rate vs. Viscosity Comparison

For the developed erosion model, the velocity of the fluid was decreased with increase in viscosity since the pump was run at a BEP. However Okita, Zhang, McLaury and Shirazi [22] ran the experiment at constant velocity. That may explain the difference in erosion rates at viscosities ranging from 5 to 50 cP.

4.4 Erosion Visualization via ANSYS Erosion Module

Erosion visualization is performed by using the ANSYS Erosion Module. For numerical calculations, the Erosion Module uses Discrete Phase Model (DPM) which solves the continuous phase in the Eulerian frame, and it applies a Lagrangian formulation for the trajectory of the discrete phase (solids).

At the rotation speed of 3600 rpm, the erosion rate on the impeller blades for the sand mixture of 1 cP fluid at the BEP is visualized by DPM. The front view of the erosion on the impeller blades is given in Figure 53.

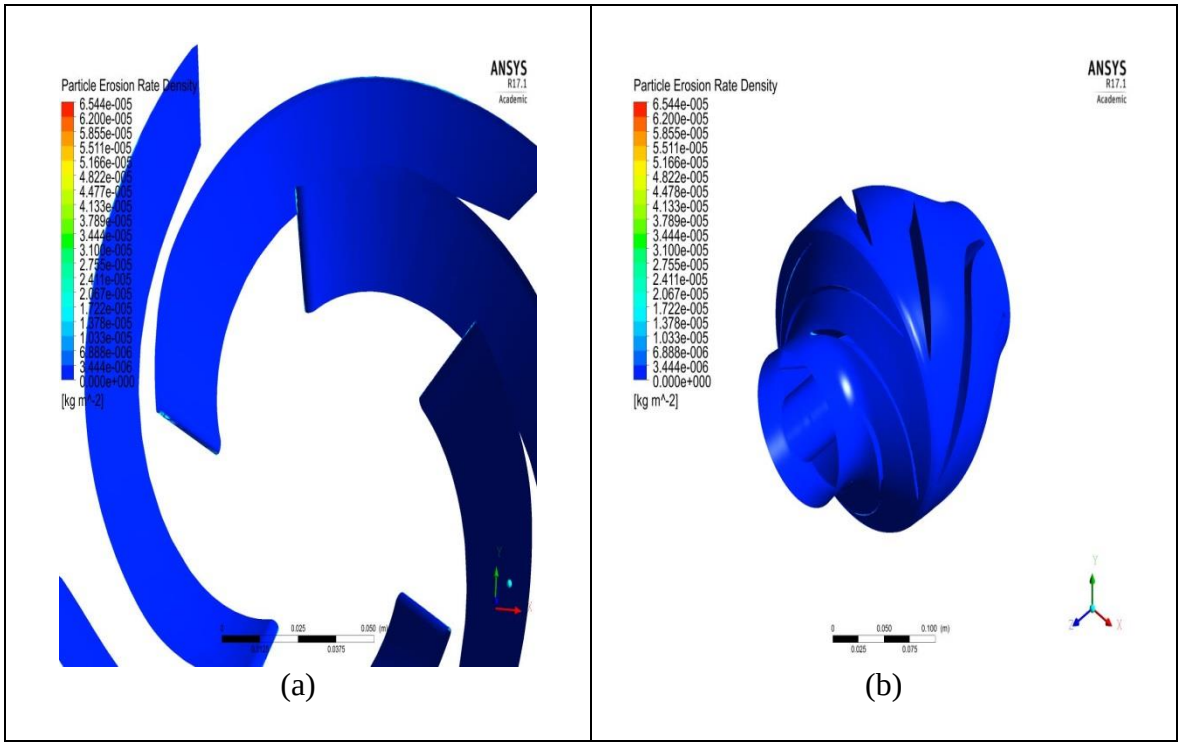

Figure 53 Erosion on the Impeller Blades (a) and Entire Pump (b) for 1 cP Fluid-Sand Mixture

Figure 53 shows that the erosion is mostly observed on the leading edges of impeller blades. The comparison of erosion rates for impeller blades obtained with both Eulerian approach and ANSYS are illustrated in Figure 54. For the legend of DPM, the maximum value of the erosion rate is decreased compared with previous figures in order to visualize the erosion better.

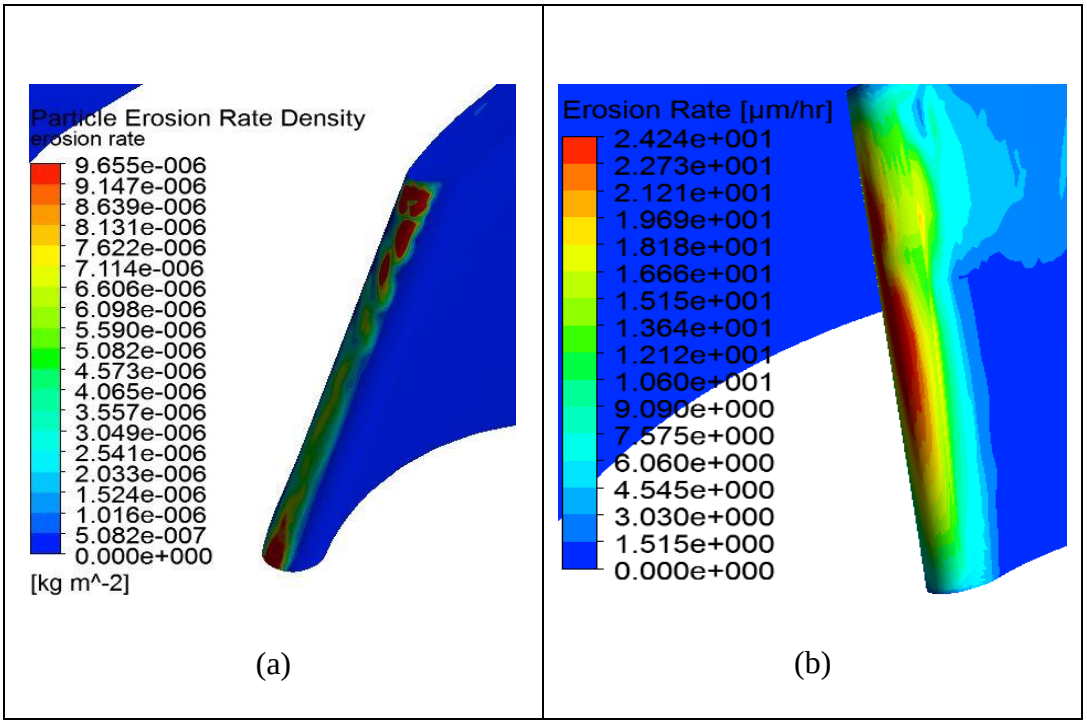

Figure 54 Erosion Rates at the Leading Edges of Impeller Blades by DPM (a) and Developed Model Using Eulerian Approach (b)

Since ANSYS Erosion Module applies discrete phase model, visualized erosion rate on the leading edges of the impeller blade is quite dense. On the other hand, relatively smooth transition was obtained by using developed model in Eulerian frame.

By using same scale of Figure 54, comparison for the back side of the impeller blades is shown in Figure 55.

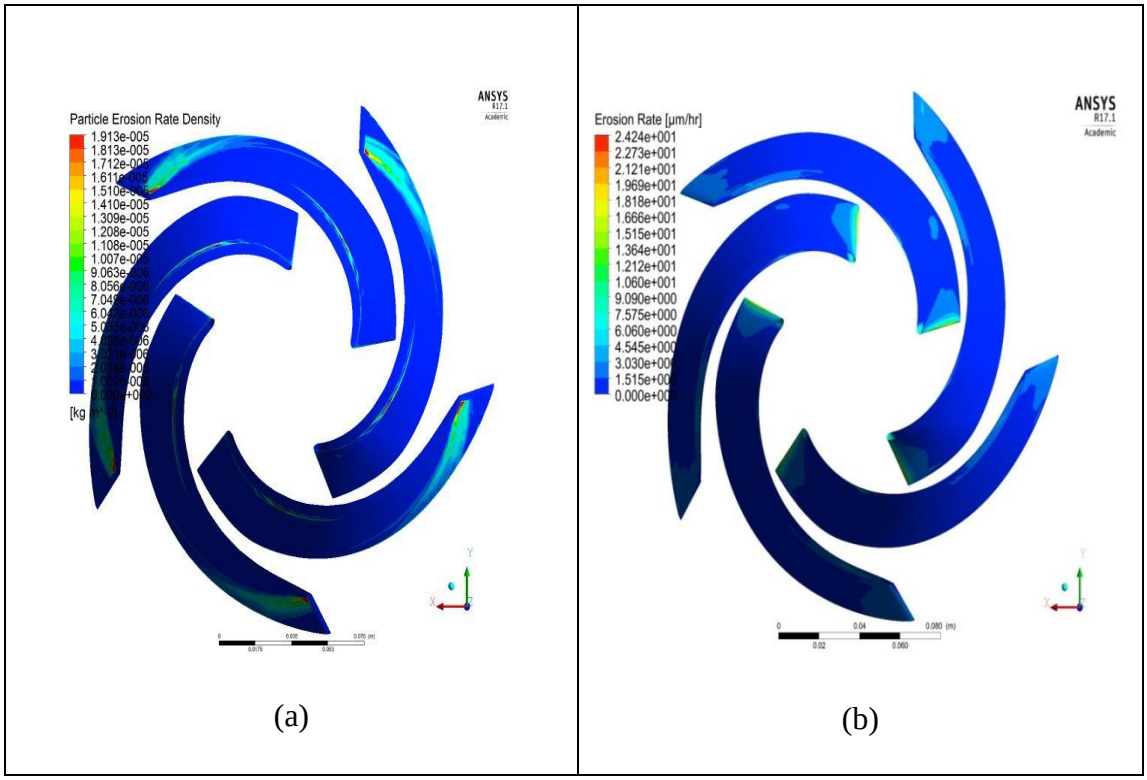

Figure 55 Erosion Rates at the Discharge Side of Impeller Blades by DPM (a) and Developed Model Using Eulerian Approach (b)

As seen, the erosion rate obtained by DPM is denser than Eulerian approach. Although the Eulerian approach shows erosion on the suction side of impeller blades, because of the narrow scale of legend, this does not make a huge difference since erosion rate is small.

4.5 Evaluation of Air Presence on ESP Erosion

Mazumder [32] developed a mechanistic erosion model to predict erosion when the flow is multiphase. Annular flow patterns were investigated since high density of erosion was observed for annular flows. The characteristic velocity of solid particles which plays a significant role on erosion was investigated. Characteristic particle velocity values were calculated independently for liquid and gas phases with the set of equations. Then, the assumption is made that gas phase is distributed homogeneously in the arrangement of discrete bubbles that move at various velocities in the liquid phase. Figure 56 shows the comparison between the mechanistic model and measured erosion for annular multiphase flow. Good agreement was obtained.

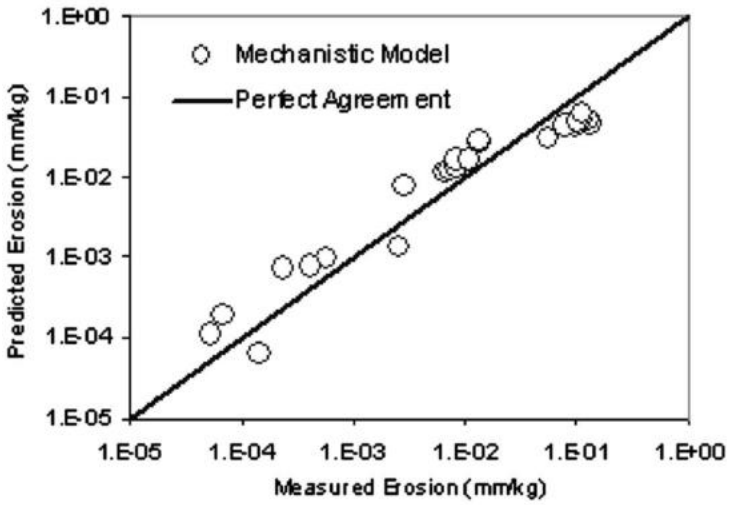

Figure 56 Measured Erosion vs. Mechanistic Model for Annular Flow [32]

Previously, water-air-sand three phase flow inside the ESP was experimentally investigated by Dezhi Zheng [28] in Turbomachinery Laboratory. 1000 GPM of volume flow rate with 15 % GVF was utilized on the pump inlet. In this study, 125 psi head was obtained for the three stages of the ESP.

In the current study, two phase flow of water and air was modelled to see the effect of air on the flow pattern. Two phase flow of water and air bubbles with different diameters were modelled to visualize the change in flow separation by air bubble diameter. Total flow rate at the impeller inlet was set to 980 GPM in order to be consistent with the previous experiments. There is no stage wise head rise data available for three phase flow testing with air. The current simulation was conducted with homogenized flow at the inlet with 10 GVF, which closely resembles the flow condition at the second stage. Balance holes and secondary flow path through front and back wear seal were excluded.

Table 12 Air Bubble Diameters for Water-Air Two Phase Flow Simulation, GVF: 10 %

Case	Air bubble diameter (inches)
1	0.0006
2	0.002
3	0.0035

Figure 57 shows the effect of bubble size on flow separation for the impeller of ESP.

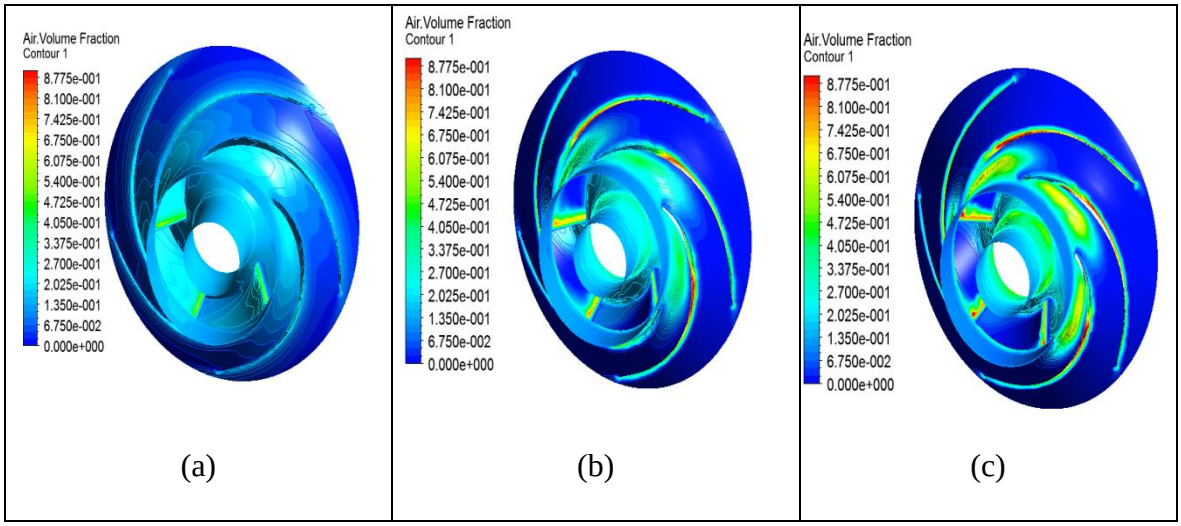

Figure 57 Flow Separation on the Impeller Hub and Blades for the Bubble Diameters of 0.0006 inches (a), 0.002 inches (b), and 0.0035 inches (c), GVF: 10%

In Figure 58, the flow separation of the entire stage for 0.0035 inches bubble diameter is illustrated.

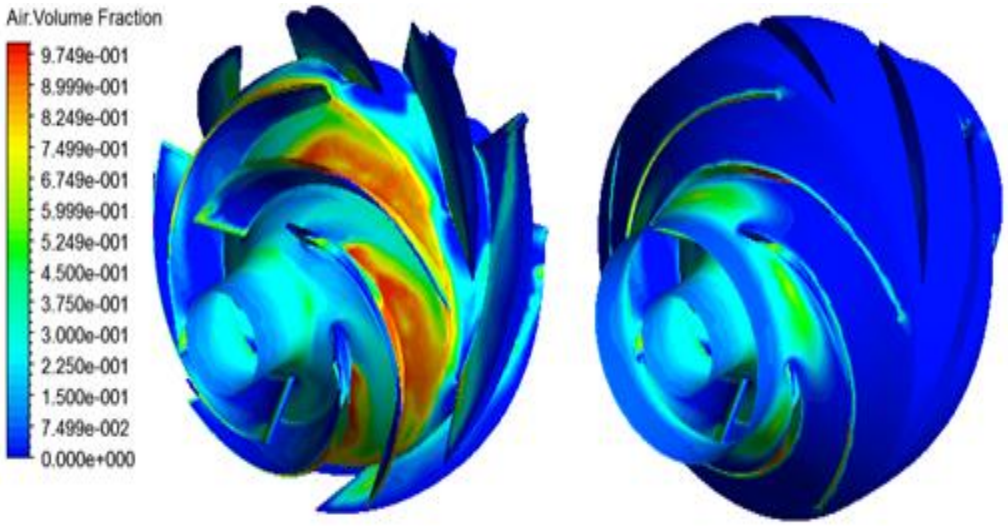

Figure 58 Flow Separation on the Entire Stage for the Bubble Diameter of 0.0035 inches

As seen in the Figure 58, increasing bubble size causes denser air volume fractions on the impeller hub surface which will lead to gas pockets. Naturally, head losses may be observed due to the presence of gas pockets. As mentioned in the literature review section, increased GVF may cause gas locking and surging conditions. At 980 GPM, when the air bubble size was set to 0.0035 inches, a 69.2 psi head rise is obtained. This pressure value found to be 75.4 psi when the working fluid was set to pure water.

CFD Simulation of Water-Air-Sand: After obtaining the two phase flow results, a new simulation is modelled for three phase flow of water, sand, and air (15 % GVF). All boundary conditions were kept the same as the two phase flow. One hundred and fifty μm sand and 0.0035 inches air bubble diameters were used in the simulations.

Blade to blade view of air presence is shown in Figure 59. The legend of the volume fractions are set to the same range for both 10 and 50 % span.

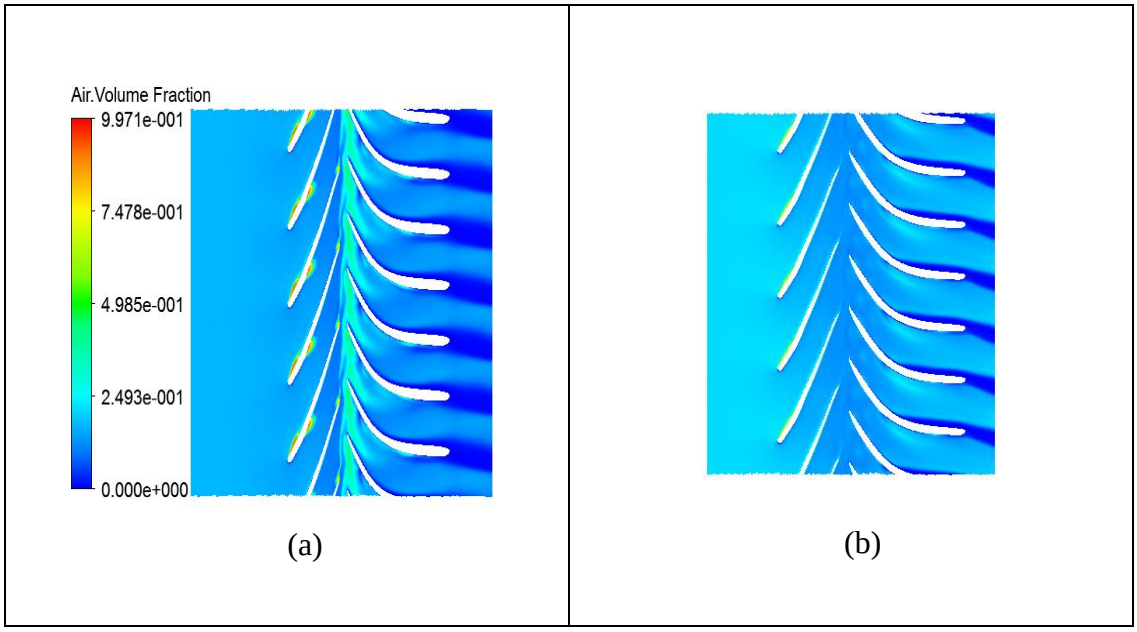

Figure 59 Gas Volume Fraction at 10 % (a) and 50% (b) Span

Air accumulation is observed near hub area and the suction side of impeller blades. The comparison of the velocity streamlines for two and three phase flow is illustrated in Figure 60.

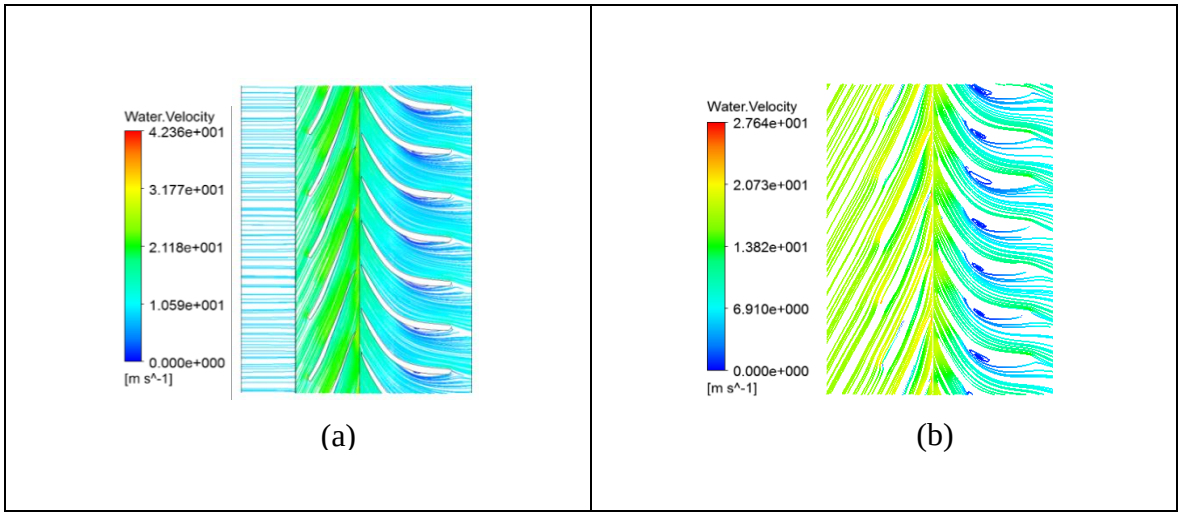

Figure 60 Velocity of Water-Sand (a) and Water-Air-Sand (b)

As seen in Figure 60, the flow tends to create recirculation on the diffuser blades for both two and three phase flows. Additionally, the separation moved towards impeller indicates reduced momentum.

In order visualize the erosion rate on the ESP, water turbulent kinetic energy which plays a key role for the developed erosion module by Pirouzpanah [26] was visualized. For the same legend scale, comparison of the TKE at the pump middle plane of two phase (water-sand) and three phase (water-air-sand) flows are shown in Figure 61.

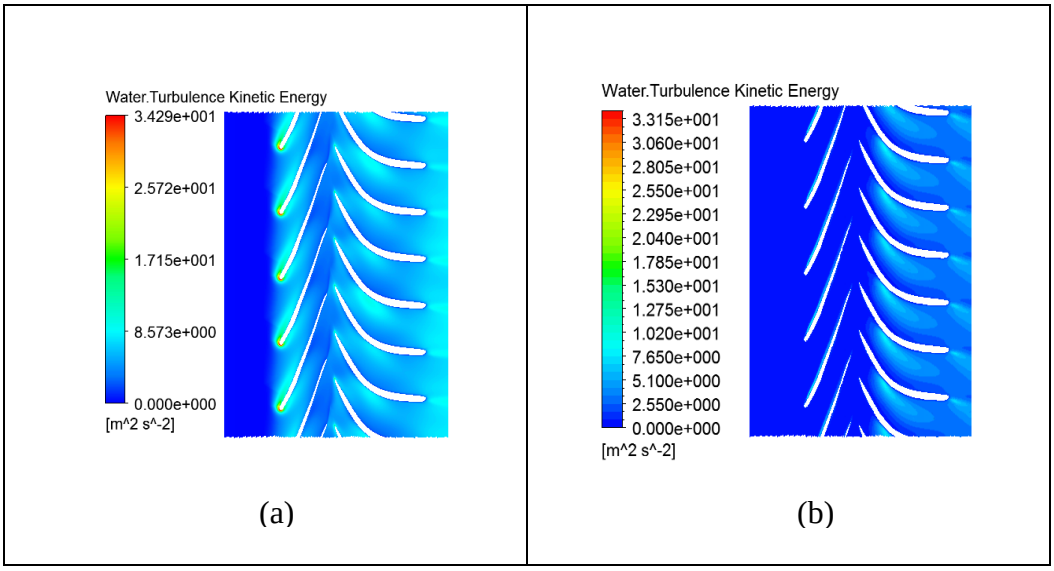

Figure 61 Comparison of TKE Distribution for Sand-Water (a) and Sand-Water-Air (b) Flow at 50% Span

The TKE distribution on the impeller section is observed very small for three phase flow when it compared with two phase flow due to air cushioning. After the TKE was obtained, the erosion rate model was applied for the three phase model. Again, comparison of erosion rates between two (water-sand) and three (water-air-sand) phase flows are visualized. Figure 62 represents the erosion rate comparison within similar erosion rate scale.

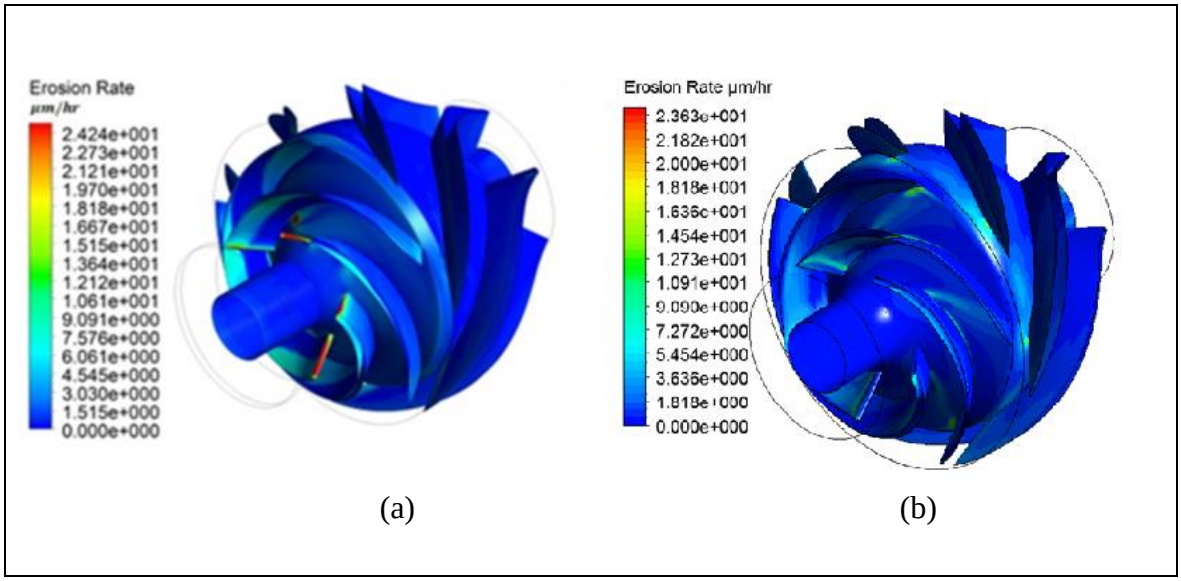

Figure 62 Comparison of Erosion Rates for Two (a) and Three Phase (b) Flows

As seen, presence of air affected the erosion rate qualitatively. A significant amount of erosion rate change is obtained on the impeller section. The closer view of Figure 62 (b) is given in Figure 63.

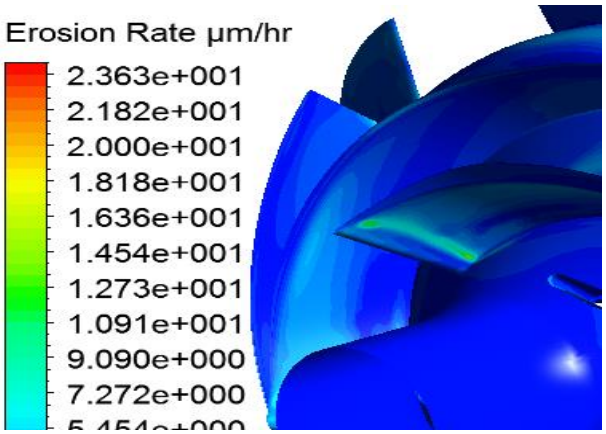

Figure 63 Erosion rate on the Leading Edges of Impeller for Three Phase Flow

For water-air-sand flow, no significant erosion is observed at the leading edges of impeller blade. The background of the developed model is based on the water turbulence kinetic energy and the sand velocity. For the three phase flow, the TKE density on the impeller section is decreased due to presence of air. Also, since the total volume flow rate is 1000 GPM, both water and sand volume flow rates, consequently velocities are decreased with respect to the BEP of the pump. These factors may explain the reason of decreased erosion rate.

Using the results of experiments performed in Turbomachinery Laboratory, pictures of eroded regions on the impeller blades are visualized in Figure 64.

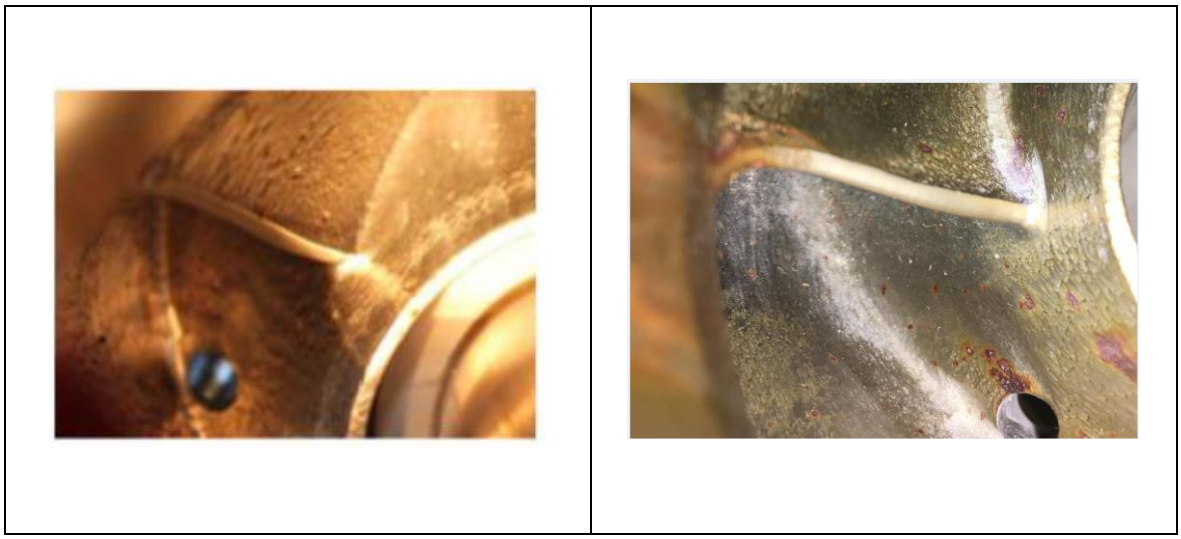

Figure 64 Wear Mark on Leading Edges of Impeller

As seen in Figure 64, similar to the simulation results, there is no dramatic change at the leading edges of the impeller section in terms of wear when air was added

to the flow zone. Applied CFD analysis using the developed model is consistent with experimental results for the leading edges.

In addition to impeller blades, as seen in Figure 62, a slightly higher amount of erosion rate is obtained on the diffuser blades for the three phase flow compared to the two phase flow. Detailed view of the obtained erosion on diffuser blades is shown in Figure 65.

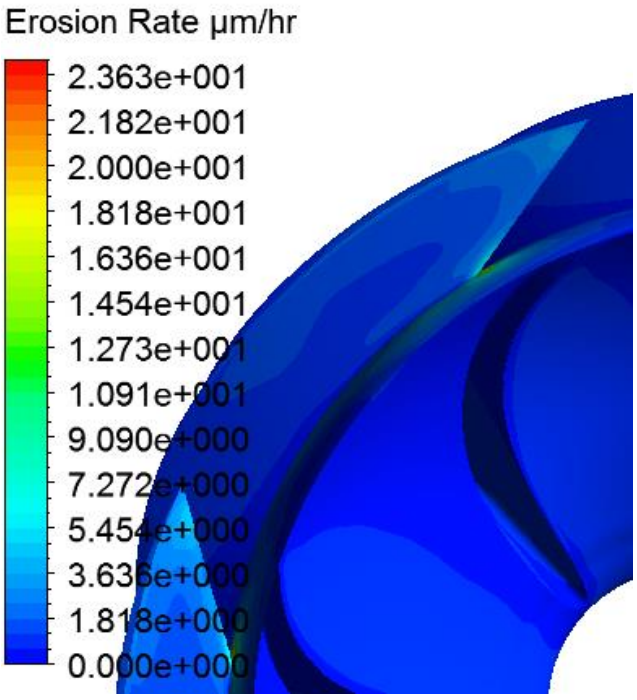

Figure 65 Obtained Erosion on the Diffuser for Three Phase Flow

However, relatively more erosion on the diffuser blades was observed on the diffuser blades using experiment results. Figure 66(a) represents the visualized erosion

on the diffuser for the first 117 hours of experiments. When the air was added into the flow zone for additional 68 hours, obtained erosion is illustrated in Figure 66(b).

(a)

(b)

Figure 66 Obtained Erosion on the Diffuser Blades by Experiments

Regarding Mazumder [32], sand particles follow the continuous phase streamlines in the bubbly flow field which means that the trend of obtained erosion between two phase (water-sand) and three phase (water-sand-air) should be similar. On the other hand, due to the high amount of GVF (15 %), sand particles may be forced to deviate from the streamlines. Presence of gas pockets may affect the water velocity on the impeller blades.

The background of the current erosion model is based on turbulence kinetic energy. The model is mainly applicable for two phase (water-sand) flows. Adding high GVF of air may affect the results. In order to visualize the influence of the bubble in the flow zone better, three phase flow with different bubble diameters should be modelled, and the erosion model should be updated regarding to results of this future study.

5. CONCLUSIONS

In this research, a computational study was carried out in order to examine the flow characteristics of an Electrical Submersible Pump. For a single stage of an ESP, the effect of viscosity and the influence of air presence on the erosion were studied. CFD simulations were performed for a single stage of the ESP. The CFD simulations were shown to be in good agreement with the pump catalog specifications and the experimental results.

The sand mixtures of four different viscosity fluids (1 cP, 5 cP, 20 cP, and 60 cP) were used for simulations. Numerical analyses were performed at the best efficiency points for each operating fluid.

Two different approaches were considered to investigate the effect of viscosity. Performing simulations in the Eulerian frame was the first method. The developed erosion model at the Turbomachinery Laboratory was utilized. The background of the developed model is based on the water turbulent kinetic energy, sand volume fraction, and near wall sand velocity. On the impeller hub and blades, decreases in the erosion rate were visualized by using higher viscosity fluids. Reasonable agreement was found between CFD predictions in this study and experimental data from previous publications.

Visualizing the erosion by using ANSYS Erosion Module, which is capable of performing numerical calculations by using both Eulerian and Lagrangian approaches, was the second method. The simulations were performed for 1 cP fluids at the pump's

BEP. The erosion rate was visualized on the impeller blades. Comparison of the ANSYS Erosion Module and the developed model was performed. Results showed a good consistency.

Three phase flow simulation was carried out using an Eulerian approach to evaluate the effect of air upon erosion in an ESP. Bubble size significantly affected the air-water separation. The current erosion model is based on incompressible single phase turbulence modeling. For the three phase flow, air bubbles with constant diameter are added to the water sand flow mixture. Fifteen percent GVF is utilized for air. The presence of air on erosion was obtained.

The recommendation for the future work is to determine the critical (highest) value of fluid viscosity which keeps the developed erosion model in the turbulent flow regime for two phase fluid-sand flow.

Constant bubble size may not reflect the actual multiphase flow characteristics in the stage. To capture precisely the effect of air presence, it is recommended to perform the three-phase simulation which can include varying bubble size in flow regime.

REFERENCES

[1] Naderi, A., Ghayyem, M. A., and Ashrafi, M., 2014, "Artificial Lift Selection in the Khesht Field," Petroleum Science and Technology, pp. 1791-1799.

[2] Flatern, R. V., 2015, "Artificial Lift," Oilfield Review 27, no.2 Schlumberger.

[3] Takacs, G., 2009, "Chapter 3 - ESP Components and Their Operational Features," Electrical Submersible Pumps Manual, Gulf Professional Publishing, Boston, pp. 51-118.

[4] Clegg, J. D., Bucaram, S. M., and Hein, N. W., 1993, "Recommendations and Comparisons for Selecting Artificial-Lift Methods(Includes Associated Papers 28645 and 29092)," Society of Petroleum Engineers.

[5] Pessoa, R., and Prado, M.,2012, "Experimental Investigation of Two-Phase Flow Performance of Electrical Submersible Pump Stages," Society of Petroleum Engineers.

[6] Gamboa, J., and Prado, M., 2011, "Review of Electrical-Submersible-Pump Surging Correlation and Models," Society of Petroleum Engineers.

[7] Lea, J. F., and Bearden, J., 1982, "Effect of Gaseous Fluids on Submersible Pump Performance," Journal of Petroleum Technology, 34(12), pp. 2,922-922,930.

[8] Turpin, J. L., Lea, J. F., and Bearden, J. L., 1986, "Gas-Liquid Flow Through Centrifugal Pumps-Correlation of Data," Proc. Proceedings of the Third International Pump Symposium, pp. 13-20.

[9] Cirilo, R., 1998, "Air-Water Flow Through Electric Submersible Pumps," University of Tulsa, Department of Petroleum Engineering.

[10] Minemura, K., and Murakami, M., 1980, "A Theoretical Study on Air Bubble Motion in a Centrifugal Pump Impeller," Journal of Fluids Engineering, 102(4), pp. 446-453.

[11] Cheah, K. W., Lee, T. S., Winoto, S. H., and Zhao, Z. M., 2007, "Numerical Flow Simulation in a Centrifugal Pump at Design and Off-Design Conditions," International Journal of Rotating Machinery, 2007.

[12] González, J., Fernández, J. n., Blanco, E., and Santolaria, C., 2002, "Numerical Simulation of the Dynamic Effects Due to Impeller-Volute Interaction in a Centrifugal Pump," Journal of Fluids Engineering, 124(2), pp. 348-355.

[13] Maitelli, C. d. P., Bezerra, F., and Mata, W., 2010, "Simulation of Flow in a Centrifugal Pump of ESP Systems Using Computational Fluid Dynamics," Brazilian Journal of Petroleum and Gas, 4(1).

[14] Minemura, K., Uchiyama, T., Shoda, S., and Egashira, K., 1998, "Prediction of Air Water Two-Phase Flow Performance of a Centrifugal Pump Based on One Dimensional Two-Fluid Model," Journal of Fluids Engineering, 120(2), pp. 327-334.

[15] Beltur, R., Prado, M., Duran, J., and Pessoa, R., 2003, "Analysis of Experimental Data of ESP Performance Under Two-Phase Flow Conditions," Society of Petroleum Engineers.

[16] Caridad, J., Asuaje, M., Kenyery, F., Tremante, A., and Aguillón, O., 2008, "Characterization of a Centrifugal Pump Impeller Under Two-Phase Flow Conditions," Journal of Petroleum Science and Engineering, 63(1–4), pp. 18-22.

[17] Qi, X., Turnquist, N., and Ghasripoor, F., 2012, "Advanced Electric Submersible Pump Design Tool for Geothermal Applications," GRC Transaction, 36, pp. 543-548.

[18] Marsis, E. G. R., 2012, "CFD Simulation and Experimental Testing of Multiphase Flow Inside the MVP Electrical Submersible Pump," Texas A&M University.

[19] Patil, A. R., 2013, "Performance Evaluation and CFD Simulation of Multiphase Twin-Screw Pumps," Texas A&M University.

[20] Amaral, G., Estevam, V., and Franca, F. A., 2009, "On the Influence of Viscosity on ESP Performance," SPE Production & Operations, 24(02), pp. 303-311.

[21] Sirino, T., Stel, H., and Morales, R. E.,2013, "Numerical Study of the Influence of Viscosity on the Performance of an Electrical Submersible Pump," Proc. ASME 2013 Fluids Engineering Division Summer Meeting, American Society of Mechanical Engineers, pp. V01BT10A026-V001BT010A026.

[22] Okita, R., Zhang, Y., McLaury, B. S., and Shirazi, S. A., 2012, "Experimental and Computational Investigations to Evaluate the Effects of Fluid Viscosity and Particle Size on Erosion Damage," Journal of Fluids Engineering, 134(6), p. 061301.

[23] McLaury, B. S., 1993, "A Model to Predict Solid Particle Erosion in Oilfield Geometries."

[24] Oka, Y. I., Okamura, K., and Yoshida, T., 2005, "Practical Estimation of Erosion Damage Caused by Solid Particle Impact: Part 1: Effects of Impact Parameters on a Predictive Equation," Wear, 259(1), pp. 95-101.

[25] Agrawal, M., 2011, "Erosion Modeling and Sand Management with ANSYS CFD," ANSYS,Inc., Houston.

[26] Pirouzpanah, S., 2014, "Experimental Measurement of Multiphase Flow and CFD Erosion Modeling in Electrical Submersible Pumps," Texas A&M University.

[27] Diaz, N. I. C., 2012, "Effects of Sand on the Components and Performance of Electric Submersible Pumps," Texas A&M University.

[28] Dezhi Zheng, G. M., 2013, "Three Phase Erosion Testing and Vibration Analysis of an Electrical Submersible Pump," Texas A&M University.

[29] Krüger, S., Martin, N., and Dupont, P., 2010, "Assessment of Wear Erosion in Pump Impellers," Proc. Proceedings of The Twenty-Sixth International Pump Users Symposium.

[30] Yin, W., 2016, "CFD Simulation of the Influence of Viscosity on an Electrical Submersible Pump," Texas A&M University.

[31] Morrison, F. A., 2013, "An Introduction to Fluid Mechanics," Cambridge University Press.

[32] Mazumder, Q. H., 2007, "Prediction of Erosion due to Solid Particle Impact in Single-Phase and Multiphase Flows," Journal of Pressure Vessel Technology, 129(4), pp. 576-582.